A multi-omics census reveals obesity-associated microRNA *miR-let-7* as novel instigator of adipose mitochondrial dysfunction and of intergenerational metabolic decline.

Chien Huang[1,2#], Joo Hyun Park[1#], Ali Altintas[3], Natasa Stanic[1], Hande Topel Batarlar[1], Rocio Valdebenito Malmros[1], Jesper Havelund[1], Nils Joakim Færgeman[1], Bjørk Ditlev Marcher Larsen[1], Karolina Szczepanowska[4,5], Jan-Wilm Lackmann[4], Aleksandra Trifunovic[4], Eva Kildall Hejbøl[6], Sönke Detlefsen[6,7], Ida Engberg Jepsen[8], Stefanie Hansborg Kolstrup[9], Ricardo Laguna-Barraza[10], Javier-Martin Gonzalez[10], Konstantin Khodosevich[11], Romain Barrès[3] and Jan-Wilhelm Kornfeld[1,12*]

[1]Department of Biochemistry and Molecular Biology (BMB), University of Southern Denmark (SDU), Odense, Denmark. [2]Laboratory of Animal Physiology, Department of Animal Science and Technology, National Taiwan University, Taipei, Taiwan. [3]Novo Nordisk Foundation Center for Basic Metabolic Research (CBMR), Faculty of Health and Medical Sciences, University of Copenhagen, Copenhagen, Denmark. [4]Cologne Excellence Cluster on Cellular Stress Responses in Aging-Associated Diseases (CECAD) & Center for Molecular Medicine (CMMC), University of Cologne, Cologne, Germany. [5]IMol Polish Academy of Sciences, Warsaw, Poland. [6]Department of Pathology, Odense University Hospital, Odense, Denmark. [7]Department of Clinical Research, Faculty of Health Science, University of Southern Denmark, Odense, Denmark. [8]The Fertility Clinic, Department of Obstetrics and Gynecology, Zealand University Hospital, Koege, Denmark. [9]Biomedical Laboratory, Institute of Molecular Medicine, University of Southern Denmark, Odense, Denmark. [10]Core Facility for Transgenic Mice, Department of Experimental Medicine, Faculty of Health and Medical Sciences, University of Copenhagen, Copenhagen, Denmark. [11]Biotech Research & Innovation Centre (BRIC), University of Copenhagen, Copenhagen, Denmark. [12]Novo Nordisk Foundation Center for Adipocyte Signaling, University of Southern Denmark, Odense, Denmark.

#These authors contributed equally to this work,

*Corresponding author

Abstract

We here describe that obesity and weight loss in male mice causes reversible abnormalities in glucose and lipid metabolism, serum metabolomes and reduced expression of genes controlling mitochondrial energy dissipation in white adipose tissue. When mating obese male mice with lean females, we observed concordant reductions in adipose mitochondrial gene expression and translation in offspring (F_1) that resemble those observed in the paternal (F_0) generation. When mapping miRNA differential expression across somatic organs and the germline (i.e., liver, adipose tissue, sperm) and generations, we found that obesity and weight loss reversible affected miRNA levels, and that *miR-let7* isoforms were induced in adipose tissues of obese F_0 and F_1 adipose tissue and sperm of obese F_0 mice. Overexpressing *miR-let-7* in adipocytes silenced DICER1, a cellular rheostat required for adipose tissue adaptation in obesity as evidenced by deficiencies in mitochondrial function following DICER1 loss in adipocytes. Delivery of *miR-let-7* into lean oocytes elicited glucose intolerance and impediments in adipose mitochondrial gene expression in mice sired from miRNA-injected embryos, thus phenocopying important aspects of obesity heredity. When performing single-cell RNA-Seq of miRNA-injected embryos, *miR-let7* impaired mitochondrial gene expression, suggesting altered energy metabolism following alterations in zygotic miRNAs. When studying miRNA alterations in human semen, lifestyle-induced weight loss downregulated *MIR-LET-7* in human subjects, suggesting similar roles for human *MIR-LET-7* in gametic epigenomes and embryogenesis.

45 **Introduction:**

46

47 ***Intergenerational epigenetic inheritance of metabolic dysfunction***

48 Genome-wide association studies have demonstrated that genetic (i.e., DNA) variants only explain 20%
49 of obesity heritability[1]. Given the pandemic rise in obesity within evolutionarily short timescales, non-
50 genetic or ‚*epigenetic*' processes, i.e., processes spurred by obesogenic lifestyles, increase disease
51 susceptibility and could contribute to obesity development. This type of epigenetic inheritance is
52 particuarly intriguing for paternal programming where fathers contribute only sperm as biological
53 material to fertilized embryos (‚intergenerational inheritance') or no genetic/biological material at all
54 (‚transgenerational inheritance'). Epidemiological support for the existence of hereditary, paternally-
55 acquired traits comes from historical records demonstrating that ample ancestral food supplies affects
56 cardiometabolic traits for up to two generations[2,3], showing that individuals carry increased risks of
57 cardiometabolic dysfunction if their parents or grandparents were obese[4]. In line with these correlative
58 observations in human, mechanistic studies in isogenic mice demonstrated that paternal obesity impairs
59 metabolism in offsprings (i.e., F_1 generation and beyond) and, for instance, low-protein[5] or high-fat diet
60 feeding[6-8], depression-like behavior[9], fear-conditioning[10] and psychological traumata[11] all impart
61 epigenetic behavioral and metabolic effects in offsprings. Recently, also beneficial types of epigenetic
62 programming were shown, and rodent offspring conceived following cold temperature exposure display
63 increased amounts of metabolically favorable brown fat[12], suggesting a high plasticity of the molecular
64 and cellular mechanisms underlying intergenerational epigenetic responses.

65

66 ***The molecular basis for epigenetic inheritance of paternal obesity in male gametes***

67 The molecular and cellular basis for epigenetic heredity remains enigmatic: Although changes in
68 epigenetic marks such as DNA methylation (DNAme), histone post-translational (PTM) modifications
69 and small Noncoding RNAs (sncRNAs) all control epigenetic processes in male gametes[13], and despite
70 lifestyle/diet-induced changes in DNAme and histone PTMs being reported, evidence for causatively
71 implicating these marks in eliciting paternal response in progeny is rare for higher organism like rodents
72 and humans. Other instigators of intergenerational response are found amongst the different types of

73 gametic sncRNAs like microRNAs (miRNAs): miRNAs were initially described in nematodes and fruit
74 flies[14-17] and sncRNAs-evoked gametic gene silencing is well-understood [18]. Due to their mobile nature
75 and microvesicular exchange between cell types[19], high abundance in gametes and dynamic changes in
76 expression following exposure to diet[20,21], sperm-derived sncRNAs have the potential for transmitting
77 lifestyle choices to zygotes and progeny. Consistent with this, metabolic trait-associated miRNAs affect
78 intergenerational phenotypes and phenocopy parts of F_0 lifestyles if microinjected [22,23] or removed from
79 zygotes[24]. Beyond controlling gametic epigenomes, miRNAs are essential for germ cell development
80 processes like spermatogenesis[25] and embryogenesis[26], and miRNA can be exchanges between zygotes
81 and other cell types [11,23,27-29]. Taken together, it is plausible to hypothesize that obesity-evoked changes
82 in sperm miRNAs alter zygotic miRNA pools and embryonic development, instigating epigenetic
83 phenotypic traits and somatic gene expression changes in offsprings. As diverse paternal lifestyle
84 exposures ranging from inflammation[14], nutrition[27,29] to stress [11,28] alter gametic miRNA repertoires and
85 F_1 phenotypes in non-overlapping ways, the intriguing possibility exists that environmental experiences
86 are encoded in individual gametic sncRNA signature and that these sperm sncRNAs have the potential
87 to transmit complex lifestyle exposures given the high bandwidth of RNA-mediated effects[30].
88
89 ***Regulation of adipose tissue (mitochondrial) function by miRNAs***
90 Adipose tissue is a multifunctional endocrine organ that coordinates tissue-level (autocrine, paracrine)
91 and system-wide (endocrine) responses by release of adipokines, lipids and inflammatory factors and,
92 shown recently, microvesicles (exosomes)[31-33]. Adipose tissue can safely store ingested nutrients as
93 lipids, although long-term calorie excess causes insulin resistance[34], aberrant gene expression in
94 adipocytes[35], vascular remodeling and immune cell infiltration[31]. Mitochondria in adipose tissue exert
95 important functions for tissue/energy homeostasis, particularly during nutrient deprivation/excess[33]:
96 Whereas brown adipose tissue (BAT) contains large numbers of mitochondria to generate heat by
97 dissipation of the electron transport chain (ETC) proton gradients[36], white adipose tissue (WAT)
98 protects from calorie overload by removing nutrients from circulation and storing as energetic
99 macromolecules. Mitochondrial function in WAT is impaired in obesity [37] and reduced mitochondrial
100 function in fat itself causes metabolic imbalance[38-41]. Mitochondrial DNA content, oxidative

101 phosphorylation (OxPhos), abundance and composition of ETC complexes are functionally impaired in
102 obesity and morphological aberrations are found in obesity[37,41] and aging[42]. Conversely, treatment with
103 AMP-activated protein kinase (AMPK) agonist Metformin improves mitochondrial function in adipose
104 tissue, as do exercise or calorie restriction, and these interventions correlate with metabolic
105 improvement[43]. MiRNAs are important regulators of mitochondrial function and *miR-143, miR-181a,*
106 *miR-378* instigate, whereas *miR-532* negatively affects mitochondrial function by post-transcriptionally
107 silencing mitochondrial translocation and RNA homeostasis[44-46]. We and others showed that removing
108 miRNAs from adipocytes by ablating DICER1, a central component of the conserved miRNA
109 processing machinery, impairs adipogenesis, thus triggering lipodystrophy and metabolic dysfunction
110 in mice[47-49].
111
112 Collectively, we here report that obesity in the male mice is linked to reversible alterations in adipose,
113 but not liver, mitochondrial gene regulation that are inherited to adipose tissue of F_1 progeny. We
114 mechanistically implicate obesity-associated *miR-Let-7*-driven suppression of DICER1 and
115 concomitant declines in mitochondrial function in adipocytes, and established sperm-derived *miR-Let-*
116 *7* as intergenerational driver of mitochondrial dysfunction and glucose impairments in F_1 offspring.

117 **Results**

118 ***Paternal obesity and weight loss elicit reversible changes in mitochondrial metabolites***

119 The epigenetic and phenotypical consequences of altering paternal metabolism by experimental high-
120 fat diet feeding have been documented, yet the plasticity of hereditary dietary effects remains elusive.
121 To investigate the potential reversibility of metabolic dysfunction in the paternal (F_0) and offspring (F_1)
122 generation, we used diet-induced obese (DIO) 6-week-old male C57BL/6J mice as rodent model. We
123 fed animals with i. low-fat diet (F_0 LF) ii. micronutrient-matched high-fat diet (F_0 HF) for 18 weeks or
124 iii. fed HF for 9 weeks, followed by 9 weeks of LF-induced weight loss feeding (F_0 HF-LF), and F_1
125 progeny sired from each group received LF to specifically interrogate the hereditary sequelæ of F_0
126 metabolism (**Fig.1a**). We found that HF-LF-evoked weight loss corrected HF-induced body weight
127 gains (**Fig.1b**), glucose intolerance (**Fig.1c,d**), insulin resistance (**Fig.1e**), and reduced serum glucose
128 (**Fig.1f**), insulin (**Fig.1g**), and leptin levels (**Fig.1h**). We examined organ/body weight ratios to evaluate
129 tissue-level effects of weight gain and regression, and found that weight loss corrected the HF-induced
130 increase in epididymal WAT (eWAT) and inguinal WAT (iWAT) mass, yet did not affect liver and
131 BAT to body weight ratios (**Fig.1i**). To gain system-level insights into the effects of obesity and weight
132 loss, we performed i. serum metabolomics ii. serum lipidomics, iii. transcriptomics (mRNAseq and
133 small RNAseq, sRNAseq) iv. proteomics and v. histological profiling in liver and eWAT of F_0 groups
134 (**Fig.1j**). By metabolomics, we detected 600 unique features (**Table S1**) that segregated animals into
135 three groups (**Fig.1k**). When focussing on metabolites that were (re)-reversibly affected by weight loss
136 **(Fig.1l)**, we found that mitochondria-associated metabolites such as the tricarbon acid (TCA) cycle
137 intermediates citrate, malate, fumarate, alpha-ketoglutarate and citrate, were reduced by obesity and
138 restored by weight loss (**Fig.1m**, **Fig.S1a,b**). Using lipidomics, we detected 117 lipid species (**Table**
139 **S2)** that correlated with body weight trajectories and were able to segragated F_0 groups (**Fig.S2a,b**).
140 Amongst these, we observed that saturated, short-chain ceramides, i.e., inhibitors of mitochondrial FA
141 oxidation in adipose tissue[50], were reversibly induced, whereas more indolent, long-chain, unsaturated
142 ceramides were reversibly downregulated by HF feeding (**Fig.S2c**). *Thus, dietary obesity and weight*
143 *loss cause reversible alterations in energy metabolism in mice that correlate with serum metabolites*
144 *that are instigators of tissue-level mitochondrial dysfunction.*

145

146 ***Obesity triggers reversible mitochondrial mRNA-miRNA gene alteration in adipose tissue.***

147 Beyond instigating mitochondrial dysfunction at the systemic metabolite level, obesity and weight loss
148 reversibly increased eWAT adipocyte size (**Fig.2a,b**) and prompted Metabolic Dysfunction Associated
149 Liver Disease (MASLD) hallmarks such as micro- and macrovasicular steatosis, fibrosis and lobular
150 inflammation (**Fig.S3a-e**). Given the pronounced lipid accumulation in adipose tissue and liver, we next
151 asked if the observed reduction in serum mitochondrial metabolites in obese mice coincided with tissue-
152 level mitochondrial dysfunction in these organs, and performed global transcriptomic profiling in liver
153 and eWAT of F_0 groups. Analysis of liver mRNAseq and group-level plotting using multidimensional
154 scaling (MDS) showed that the F_0 LF group segregated from others (**Fig.S3f**). When comparing F_0 HF
155 vs F_0 LF, we found 3,495 up-regulated and 1,639 down-regulated genes (**Fig.S3g**), mirroring the effects
156 observed when comparing F_0 HF-LF vs F_0 LF that yielded 3,095 up-regulated and 955 down-regulated
157 genes (**Fig.S3h**). Conversely, comparing F_0 HF vs F_0 HF-LF, yielded only 808 up-regulated and 960
158 down-regulated genes (**Fig.S3i**), highlighting that the expression changes triggered by HF feeding in
159 liver were to large parts irreversible despite the profound weight loss (**Table S3**). Gene Set Enrichment
160 (GSEA)[51] analyses of differentially expressed genes (DEG) revealed upregulated processes such as lipid
161 metabolism and organelle formation, whereas repressed processes include lipoprotein trafficking,
162 endoplasmatic reticulum and ribosome function (**Fig.S3j**), yet we observed no transcriptional evidence
163 of altered mitochondrial processes. Next, we turned our attention to adipose tissue and performed
164 RNAseq followed by DEG analysis (**Table S4)**. MDS analysis showed transcriptional segregation of
165 diet groups (**Fig.2c, Fig.S4a**) and, comparing F_0 HF vs F_0 LF, we found 2,337 up-regulated and 3,867
166 down-regulated genes (**Fig.2d)**. These effects that were to a large degree reversible, as evidenced by
167 analysing the comparison between F_0 HF vs F_0 HF-LF that yielded 1,986 up-regulated and 2,858 down-
168 regulated genes (**Fig.2e**), whereas the comparision F_0 LF and F_0 HF-LF mice only yielded 262 up-
169 regulated and 459 down-regulated genes (**Fig.2f**). When performing GSEA on DEG we found gene
170 ontology (GO) processes related to cell proliferation and immune activation; known transcriptional
171 processes reflecting adipocyte hyperplasia and inflammation associated with obesity. Importantly, we
172 also detected GO terms related to lipid catabolism, mitochondrial ATP synthesis and respiration and

173 ETC downregulated in obese adipose tissue (**Fig.2g**). When specifically interrogating the expression of
174 mRNA encoding ETC Complexes I-V, we confirmed the pervasive repression of nuclear-expressed
175 ETC mRNAs (**Fig.S4b**).
176
177 The down-regulation of mitochondrial programs in obese eWAT at least prompted the question whether
178 mitochondria-associated ‚mito-miRs[1]' like *miR-let-7*[2], *miR-378*[3], *miR-181*[4], *miR-143*[5] that are known to
179 support mitochondrial formation and bioenergetics, contribute to these effects. When thus conducted
180 small RNA-Seq (sRNAseq, **Table S5**) and found profound changes between F_0 adipose miRNomes
181 (**Fig.2h**). As expected, mito-miRs promoting mitochondrial biogenesis and function, for instance *miR-*
182 *143-3p*, *miR-181a-2-3p*, *miR-378a-3p* and *miR-378* where (reversibly) repressed, whilst mitochondria-
183 inactivating *miR-532* was reversibly induced in F_0 HF eWAT (**Fig.2i**), suggesting that miRNA
184 deregulation contributed to the observed mitochondrial impediments observed in obese fat. Integration
185 of our miRNA-mRNA datasets with miRNA-mRNA interactomes from fat-specific AGO-HITS-CLIP[6]
186 confirmed that HF-associated mito-miRs might be an important driver of the mitochondria dysfunction
187 observed in obese eWAT (**Fig.2j**). *Thus, obesity caused a pervasive, reversible repression of*
188 *mitochondrial ETC genes, FA oxidation and OxPhos, and miRNA-mRNA network analysis implicates*
189 *obesity-repressed mito-miRs in this process.*
190
191 ***Paternal obesity causes concordant mitochondrial changes in offspring adipose tissue.***
192 Unresolved questions in the field of epigenetic phenotypic inheritance revolve around the 'bandwidth'
193 and 'plasticity' of heritable intergenerational responses: Whilst the former tries to answer if paternal
194 hereditary processes like fear conditioning[7], temperature homeostasis[8], and adipose activation can elicit
195 concordant molecular, metabolic and behavioral alterations in offsprings [9], 'plasticity' refers to the
196 reversibility of paternally acquired and inherited traits. To address both points, we next mated lean,
197 obese and weight-regressed male mice with lean virgin female mice. Following mating, female mice
198 gave risen to three offpspring generations: F_1 of F_0 LF (n=44), F_1 of F_0 HF (n=52), and F_1 of F_0 HF-LF
199 (n=38) and average litter sizes (7.33, 5.7, 6.33, respectively) and rate of successful matings (100%,

200 75%, 100%, respectively) were not different between groups whilst gender ratios differed (i.e., 58.7%,
201 57.7%, 45.5% being female mice, respectively).
202
203 To interrogate physiological and molecular effects of ancestral diet feeding without confounding HF
204 challenges, F_1 offsprings groups were fed only LF; and body weight in F_1 groups did not differ (**Fig.3a**).
205 In contrast, progeny sired by obese father exhibited glucose intolerance (**Fig.3b,c**) and impaired insulin
206 sensitivity (**Fig.3d**) despite similar random-fed glycemia and serum insulin levels (**Fig.3e,f**).
207 Intriguingly, offsprings of fathers undergoing pre-conception weight loss (i.e., the F_1 [F_0 HF-LF] group)
208 did not exhibit metabolic aberrations, highlighting that intergenerational responses are plastic and thus
209 reflect dynamic changes in paternal lifestyle and metabolic improvement. Concurrently with aberrations
210 in glucose metabolism, F_1 [F_0 HF-LF] mice had higher serum leptin adipokine levels (**Fig.3g**), trended
211 towards increased fat mass (**Fig.3h**), and exhibited higher relative eWAT tissue weight (**Fig.3i**), and
212 adipocyte hypertrophy (**Fig.3j,k**), ressembling the adipose effects seen in F_0 HF mice. Prompted by the
213 reversible eWAT-hypertrophy in F_1 mice, we next performed RNAseq in eWAT of F_1 groups: Although
214 calculation DEG of transcriptional changes using similar statistical stringencies as in F_0 yielded only
215 few DEG (**Fig.S5a**), GSEA demonstrated reversible induction in germ cells-associated processes,
216 whereas mitochondrial processes were reversibly repressed in eWAT of F_1 [F_0 HF] mice (**Fig.3l**) and
217 similar patterns of ETC complex I-V (CI-IV) gene repression were observed as in F_0, albeit with less
218 robust statistical significance and smaller effect sizes (**Fig.S5b**), yet qualitatively mimicking gene
219 changes observed in the F_0 HF-LF fathers themselves. To interrogate if these transcriptional changes
220 caused biologically meaningful changes in mitochondrial proteins, we conducted bulk proteomics by
221 mass-spectrometry in eWAT of F_0 and F_1 groups (**Fig.3m**) and found an enrichment of mitochondrial
222 GO processes in downregulated cluster II (**Fig.S7a**), validating repression of important ETC proteins
223 NDUFA6, COX6B1 (**Fig.3n**) and NDUFA8, NDUFS6, and mitochondrial FA carrier proteins like
224 Carnithin Palmitoyltransferase 1 (CPT1, **Fig.S5c**) in F_0 HF and F_1 [F_0 HF-LF] eWAT. Of note, mRNA-
225 seq experiments in F_1 livers did not yield similar transcriptional (i.e. mitochondria-associated, reversible
226 by weight loss) and morphological (HF-induced cellular hypertrophy) sequelæ of paternal obesity
227 (**Fig.S6a-j**), emphasizing the specificity of paternal programming and metabolic and mitochondrial

228 decline for epididymal adipose tissue. *Thus, we here demonstrate decreased glucose homeostasis and*
229 *adipose hypertrophy in mice sired from obese fathers which was corrected by paternal pre-conception*
230 *weight loss, and that correlated with hereditary patterns of mitochondrial dysfunction in adipose tissue.*
231
232 ***Paternal obesity reversibly affects the germeline miRNome and induces miR-let-7 in F_0 and F_1.***
233 One particularly abundant molecular entity in male germ cells (spermatozoa) are various sncRNAs such
234 as miRNAs, transfer RNA (tRNA) fragments[24] and, recently, mitochondrial mt-RNA-derived cleavage
235 products[21]. As small RNAs are subject to dietary cues in humans[20], it is conceivable that diet can alters
236 spermatic miRNAs which, following fertilisation, are transferred into oocytes and affect zygotic and
237 embryonic development, thereby contributing to the altered phenotypic traits and gene expression we
238 observed in offspring from obese fathers.
239
240 To test the effects of obesity and weight gain on male gametic miRNAs, we next isolated motile sperm
241 by swim-up assays, and mapped F_0 sperm as well as F_0 and F_1 eWAT miRNA alterations by sRNA-Seq
242 (**Fig.4a,Fig.S7b**). Amongst miRNAs induced in F_1 eWAT, we did not observe mito-miR deregulation
243 as for F_0 eWAT (**Fig.S7c**) argueing against their causatively involvement in heritable mitochondrial
244 dysfunction. In contrast, by focussing on miRNAs that were concurrently regulated in F_0 and F_1, we
245 detected *miR-let-7* family members induced in F_0 sperm, and F_0 and F_1 eWAT (**Fig.4b,c**;**Fig.S7d**). *miR-*
246 *let-7* has been described in intergenerational obesity studies by us [7] and others[52], and is known to impair
247 embryo implantation and glucose homeostasis when overexpressed [53,54]. Amongst *miR-let-7* isoforms,
248 *miR-let-7d-5p* and *miR-let-7e-5p* were consistently induced across generations (F_0, F_1) and in spermand
249 eWAT (**Fig.4c**), so chose to functionally dissect their role in sperm and eWAT.
250
251 *miR-let-7i* has also been described in the context of adipocyte differentiation[55], yet its roles in
252 mitochondrial homeostasis of mature adipocytes are unreported . To mimic the obesity-associated
253 increased in *miR-let-7d/e-5p in vitro*, we delivered mature miRNA mimetics by reverse transfection of
254 stromal vascular fraction (SVF)-derived epididymal white adipocytes (1°eWA, **Fig.4d,e**). When we
255 interrogated the effects of ectopic *miR-let-7* delivery by mRNAseq, we found that both *miR-Let-7*

256 isoforms triggered similar transcriptional effects 1°eWA as expected owing to their similar nucleotide
257 sequence (**Fig.S8a**). Compared to Negative Control (NC) oligonucleotides, *miR-let-7d-5p* caused more
258 pronounced changes (977 down-regulated, 1,301 up-regulated DEG) than *miR-let-7e-5p* (759 down-
259 regulated, 635 up-regulated DEG) and both downregulated GO processes related to lipid metabolism,
260 Insulin-AKT Serine/Threonine Kinase (AKT) signaling and carbohydrate metabolism (**Fig.4f,g,**
261 **Fig.S8b**). To test if these gene expression changes also affect mitochondrial function, we predicted *miR-*
262 *let-7* target gene networks using AGO-HITS-CLIP datasets [56]and found that *miR-let-7* induction in
263 eWAT was linked to repression of several MitoCarta 3.0-annotated mitochondrial genes (**Fig.4h,Table**
264 **S8**). Amongst a wider range of predicted targets, we validated *miR-let-7* mRNA targets linked to
265 mitochondrial FA uptake (*Slc25a24*), glycolysis (*Hk2*, *Pdk2*) and miRNA processing (*Dicer1*) using
266 dual luciferase reporter assays (DLRA)-based miRNA-mRNA interaction studies in HEK293 cells
267 (**Fig.4i**). We found that *Dicer1* 3'UTRs harboured two independent *miR-let-7* seeds (**Fig.4h**) that, upon
268 mutation, became refractory to *miR-let-7* repression (**Fig.4j**). As 1°eWA overexpressing *miR-let-7d/e-*
269 *5p* reduced DICER1 protein, but only caused mild reductions in mitochondrial/TCA-associated protein
270 itself (**Fig.4k**,**Fig.S8c,d**), we hypothesized that the chronic *miR-let*-7 induction seen in obesity might
271 repress mitochondrial function via sustained DICER1 loss; and that *Dicer1* silencing is a better proxy
272 for mimicking the prolonged *miR-let-7d/e-5p* induction in obesity. To test if *Dicer1* knockdown can
273 phenocopy the obesity-induced impairment in adipocyte mitochondrial function, we next designed two
274 *Dicer1*-targeting locked nucleic acid (LNA) oligonucleotide inhibitors that repressed *Dicer1* (**Fig.S8e**)
275 and protein (**Fig.S8f**) and interrogated mitochondrial function using Seahorse bioenergetics in *Dicer1-*
276 deficient 1°eWA. We found that *Dicer1* silencing repressed oxygen consumption rates (OCR, **Fig.4k**)
277 as proxy for OxPhos activity, and reduced extracellular acidification rates (ECAR) which reflects lactate
278 production as proxy for glycolytic rates in 1°eWA (**Fig.4l**). *Thus, paternal obesity changes miRNA*
279 *expression in germline and somatic tissues and obesity-associated miR-let-7 impairs mitochondrial*
280 *oxidative respiration by silencing of DICER1 in mature adipocytes.*
281
282 ***Zygotic delivery of miR-Let-7 impairs glucose tolerance and adipose mitochondrial gene expression***
283 ***in sired offsprings.***

284 Prompted by the profound, yet reversible effects of obesity and weight loss on sperm miRNAs, we next
285 aimed to test the functional relevance of sperm-evoked *miR-let-7* changes for offspring phenotypes, as
286 environmentally induced and artificial alterations in sperm and zygote miRNA pools were previously
287 shown to trigger metabolic abnormalities in progeny[23,57]. We focussed on *miR-let7d/e-5p* given their
288 concordant increase in F_0 and F_1 eWAT as well as in F_0 sperm, and because *miR-let-7* is essential for
289 embryonic fate decisions[58] which partially dependent of post-transcriptional silencing of *Dicer1*[59]. To
290 test if zygotic delivery of *miR-let-7* in itself triggers phenotypical changes in F_1 that resemble those seen
291 as consequence of paternal F_0 obesity, we injected 50 femtomol of Negative Control (NC)
292 oligonucleotides, miRNA mimetics encoding *mmu-miR-let7-d/-e-5p* and *mmu-miR-699-5p* and *miR-*
293 *699a*-5p, a miRNA that was expressed at similar levels as *miR-let7-d* in sperm, but not regulated by HF
294 feeding, into zygotes conceived from lean males and females using public protocols[27] (**Fig.5a**). We
295 injected 126/138/110/106 zygotes with NC, *miR-let-7d-5p*, *miR-let-7e-5p* and *miR-699a-5p*,
296 respectively, and observed similar implantation rates, litter sizes and successful pregnancies (**Table S9**).
297 When analysing at least 19 pups per group from at least four pregnancies per group, we observed no
298 differences in BW(**Fig.5b**), relative eWAT (**Fig.5c**) and liver weights (**Fig.5d**) between F_m groups.
299 When interrogating random-fed glucose levels, we observed significant increases in progeny sired from
300 *miR-let-7d-5p*, *miR-let-7e-5p* and *miR-699a-5p*-injected embryos (**Fig.5e**). Importantly, we observed
301 impaired glucose tolerance only in mice sired from *miR-let-7d/e-5p*-injected embryos (**Fig.5f-h**) and
302 mRNA-seq profiling in eWAT, despite mild DEG changes, revealed down-regulation of mitochondrial
303 GO processes in these mice. *Thus, zygotic microinjection of miR-let-7 isoforms that accumulate in obese*
304 *sperm, causes glucose intolerance and impairment of mitochondrial gene regulation in mice derived*
305 *from these embryos.*
306
307 ***Obesity-associated miR-let-7 rewires mitochondrial metabolism during embryogenesis.***
308 Intergenerational epigenetic programming in isogenic rodent background has been reported before, yet
309 it is elusive if these effects are translatable to species with different reproductive apparatuses, genetic
310 backgrounds, and timescales of obesity development such as humans. Although epidemiological
311 evidence[3,60] suggests heritable effects in humans ('Dutch Hunger Winter'[61]), direct epigenetic effects

312 are difficult to delineate. It is becoming appreciated though, that human sperm is sensitive to nutritional
313 changes, and that nutritional and metabolic cues are sufficient to shape human sncRNA expression[20].
314 To test the effect of voluntary weight loss in semen in a cohort of (n=15) morbidly obese (BMI, 39.49
315 ± 1.80) men undergoing voluntary weight loss[62], we quantified *HSA-MIR-LET7D/E* using TaqMan
316 assays. We found that changes in *HSA-MIR-LET7D/E* correlated with weight loss (ΔBMI), suggesting
317 similar correlations between metabolic status and MIR-LET-7D/E in human and mice (**Fig.6a,b**).
318
319 As miRNA pertubation in sperm i. gives rise to incompletely developed embryos, suggesting roles for
320 sperm-derived miRNAs in embryonic development [19,63,64] and ii. zygotes can differentiate potential into
321 virtually any cell type, early zygotic / embryogenesis represents an important window of developmental
322 plasticity that might affect offspring phenotypes if perturbed. It is thus tenable that alterations in sperm
323 miRNAs change zygotic miRNA pools, which will have far-reaching consequences causing changes to
324 epigenetic and metabolic pathways in embryos[64]. Based on the observd mild but specific mitochondrial
325 alterations in F_m mice, we hypothesized that *miR-let7d/e* might inflict gene alterations during cell fate
326 decisions during embryo development, we repeated the miRNA injections, allowed miRNA-injected
327 embryos to divide until the 8-cell stage, dissociated embryos into single blastomeres, and performed
328 using custom made single-cell RNA-Seq using Smart-seq2 protocols[65] (**Fig.6c**). We found that, after
329 three cell divisions, the miRNA-injected blastomers were still transcriptionally distinct, reflecting the
330 profound transcriptional and developmental effects of perturbing miRNA in zygotes (**Fig.6d**). When
331 performing GSEA analysis of miRNA-induced DEG genesets, we found that *miR-let-7d* repressed GO
332 terms linked to mitochondrial processes such as ATP synthesis, TCA cycle and ETC/CI biogenesis.
333 Thus*, zygotic delivery of obesity-associated miR-let-7d-5p epigenetically rewires embryogenesis and*
334 *impairs mitochondrial gene regulation in blastomeres.*

335 **Discussion:**

336 ***High transcriptional plasticity of mitochondrial dysfunction in adipose tissue:***

337 In our study we found that hepatic expression changes inflicted by HFD feeding where to a large extend
338 irreversible, whereas adipose tissue miRNA/mRNA transcriptomes and translatomes, and particularly
339 mitochondrial OxPhos and TCA genesets, reverted to a state *ante*. Similar studies have investigated the
340 effects of reversible (i.e., diet- and exercise-evoked weight gain and loss) on hepatic and adipose
341 transcriptomes: Gonzalez-Francesa et al. observed[40] that sustained diet-induced weight loss correlated
342 with appreciable adipose transcriptional plasticity and mitochondrial gene expression, where short-
343 term, exercise induced did not. Thus, durations of weight loss, and differences in control diet exposure
344 might reflect the importance of nutritional and exposure factors during weight loss interventions on
345 tissue responses in obesity. Despite not performing profiling of chromatic accessibility, transcriptional
346 factor (TF) binding site enrichment analysis revealed that transcriptional activities of mitochondrial
347 biogenesis factors like Nuclear Respiratory Factor 1 (*Nrf1*) and expression of transcriptional (co)-
348 regulators such as Peroxisome proliferator-activated receptor gamma coactivator 1-alpha (*Ppargc1a*)
349 and *Nrf1*[66] were repressed in obese fat (not shown). As Brandao et al. reported [67] that ablation of
350 DICER1 in adipocytes repressed *Ppargc1a*/*Nrf1*, we can conceive a scenario where reduced DICER1
351 (for instance due to increased *miR-let-7d/e-5p*) drives and/or synergizes with reduced *Ppargc1a*/*Nrf1*
352 levels to impair mitochondrial biogenesis in hypercaloric adipocytes.

353

354 ***Reprogramming of embryonal development by gametic miRNAs:***

355 In *C. elegans* and *D. melanogaster*, germline gene silencing by small Noncoding RNAs (sncRNA) is
356 well-understood and similar processes are suggested for mammals [18]. miRNAs are not only critical for
357 sperm cell formation [25] and embryogenesis [26], but can also be transferred from sperm to zygotes and it
358 is plausible that oocyte-sperm fusion alters zygotic miRNA pools, affect embryonic development, and
359 instructs phenotypic traits and somatic gene expression in offspring as observed in our intergenerational
360 paradigm. In contrast to DNA-intrinsic epigenetic modifications like DNA methylation (DNAme) and
361 histone post-translational modifications, miRNAs diffuse between and across cellular compartments,
362 are highly abundant in most cells, and, crucially, can be exchanged between cells through extravesicular

363 transport [30]. As mature sperm is transcriptionally inert, and no mechanism exists how sperm senses
364 endocrine information and translates this into differential miRNA levels, sperm relies on 'decoding
365 somatic cell types' that possess these sentinel features and are capable of instructing sperm by transfer
366 of miRNAs and other sncRNAs like mitochondrial tRNA fragments that are exchanged between sperm
367 and oocyte at fertilisation [21]. Furthermore, epididymal cells, somatic epithelial cells of the extragonadal
368 male reproductive tracts, secrete *epididysomes*, microvesicles that fuse with nascent sperm [68], and as
369 we observed several miRNAs condordantly regulated in F_0 adipose tissue and sperm, horizontal miRNA
370 transfer from adipocytes to sperm, potentially via epididysomes is a plausible scenario that still lacks
371 experimental proof in our paradigm. Finally, altering miRNA levels like *miR-199a-5p* in zygotes by
372 microinjection is sufficient to reprogram embryonal metabolism [69], highlighting that miRNA alterations
373 can rewire embryonal development and metabolism which are still compatible with fetal development.

374 **Methods:**

375

376 ***Mice***

377 All animal experiments were approved by the Ministry of Environment and Agriculture Denmark
378 (Miljø- og Fødevarestyrelsen), the license no. 2018-15-0201-01544. All mice were housed under a 12-
379 h light/ 12-h dark cycle in a temperature and humidity-controlled facility and had *ad libitum* access to
380 diets and drinking water. 4-week-old C57BL/6J male mice (Janvier Labs) were fed with a chow diet
381 (NIH-31, Zeigler Brothers Inc., 8% calories from fat) for 2 weeks of acclimatization and then were fed
382 with either a low-fat diet (LF, D12450J, 10% kcal from fat, Research Diet) or a high-fat diet (HF,
383 D12492, 60% kcal from fat, Research Diet) for 9 weeks. After 9 weeks of feeding, half of HF-fed mice
384 were randomly assigned to the diet regression group which was given LFD.

385

386 ***Mouse husbandry***

387 All male virgin mice were maintained on the assigned diet until 21 weeks of age and mated with 10-
388 week-old C57BL/6J female virgin mice (Janvier Labs). 8-week-old C57BL/6J female mice were fed
389 with a chow diet for 2 weeks of acclimatization and then were fed with LF during breeding and lactation.
390 Mating was set up for 5 days in a female's cage and vaginal plugs were checked every morning. All
391 mice, including the F_0 HF group, were maintained on LF during breeding to remove confounding effects
392 from maternal diets. Males were sent from breeding cages to the original cage to be fed with the assigned
393 diet for additional 2 weeks and then sacrificed. The offspring from all groups of founders consumed
394 only LF. Representative male offspring from six litters per group were included in all analyses.

395

396 ***Intraperitoneal glucose and insulin tolerance tests:***

397 Mice were fasted for 6 h for glucose-tolerance tests. Fasting glucose levels were measured and then
398 mice were intraperitoneally injected with 2 g/kg body weight of 20 % glucose solution (B. Braun
399 Medical A/S). For intraperitoneal insulin-tolerance tests, random-fed glucose levels were measured,
400 and mice were intraperitoneally injected with 0.75 IU/kg body weight of 100IU stock insulin (Novo

401 Nordisk). Blood glucose levels were measured at 15, 30, 60, 90, and 120 min after injecting glucose or
402 insulin using a CONTOUR®NEXT glucometer (Bayer).
403
404 ***Dual-energy x-ray absorbance:***
405 Fat and lean mass were measured by Dual-energy x-ray absorbance (DXA) scan (PIXImus 2, GE Lunar
406 Corp.). Mice were anesthetized by isoflurane inhalation and placed in a prone position with all four
407 limbs stretched out. All body composition was measured on the total body excluding the head and tail
408 by version 2.10.041 of the proprietary software.
409
410 ***Tissue collection:***
411 Mice were sacrificed by carbon dioxide euthanasia. Livers, eWAT, iWAT and BAT were weighed,
412 snap-frozen in liquid nitrogen, and stored in -80 °C. Pieces from liver and eWAT were fixed in 4%
413 paraformaldehyde (PFA) for histology analysis. For serum collection, blood collected by the cardiac
414 puncture was centrifuged at 2,000 g for 15 min. The supernatant was collected and stored in -80 °C.
415
416 ***Sperm collection:***
417 Mature sperm cells were collected from the cauda epididymis. Briefly, sperm cells are allowed to swim
418 out from the cauda epididymis and incubate in PBS at 37 °C for 15 min. Supernatant containing sperms
419 was passed through a 40-µm cell strainer and then incubated in a somatic cell lysis buffer (0.5 % Triton-
420 X and 0.1 % SDS) for 40 min on ice. Sperms were centrifuged at 600 g for 5 min and the pellets were
421 washed with PBS and pelted again at 600 g for 5 min. The supernatant was discarded, and the pellets
422 were snap-frozen in liquid nitrogen and stored at -80 °C.
423
424 ***Zygotic miRNA microinjection and embryo implantation:***
425 Ovulation of prepubescent (4-week-old) C57BL/6J females was induced by intraperitoneal injection of
426 PMSG, 5 IU/female, followed by IP injection of hCG, 5IU/female, 47h later. After the second injection,
427 females were set in breeding with C57BL/6J stud males. Next morning, they were monitored for
428 formation of a vaginal plug (indicating mating has occurred during the night). Females were euthanized

429 and oviducts were dissected to harvest the cumuli containing zygotes and unfertilized oocytes. Cumuli
430 were disaggregated by incubation in a 10mg/ml solution of Hyaluronidase (Sigma-Aldrich ref. H4272)
431 in M2 medium (Sigma-Aldrich ref. M7167) at RT for 10 minutes. Zygotes were sorted out, assessed by
432 the presence of the second polar body and cultured in KSOM medium (Merck Millipore ref. MR-106-
433 D). Oocytes were discarded.
434
435 Each miRNAs was diluted at 10 ng/ul in microinjection buffer (5 mM Tris, 0.1 mM EDTA, pH 7.4) as
436 stock solution and kept at -80 °C. The day of microinjection, 1,5 ng/ul solutions were prepared from
437 the stock, and injected in the pronuclei of the zygotes following standard microinjection procedures.
438 Injected zygotes were cultured in KSOM until the microinjection session was completed and then
439 cryopreserved by the "Slow Freezing" Method (Manipulating the Mouse Embryo, a Laboratory Manual,
440 fourth edition, Chapter 16, Richard Behringer et al. Cold Spring Harbor Laboratory Press, 2014) and
441 transported to SDU at -150 °C for embryo transfer and recovery.
442
443 The frozen microinjected embryos were thawed at SDU and cultured in KSOM (Merck, MR-121-D)
444 for 40 minutes (Manipulating the Mouse Embryo, a Laboratory Manual, fourth edition, Chapter 16,
445 Richard Behringer et al. Cold Spring Harbor Laboratory Press, 2014). Viable embryos with intact zona
446 pellucida were selected for further transfer. These embryos were then washed in 10 drops of M2 and
447 surgically transferred to the oviducts of 0.5 dpc pseudopregnant females. Pseudopregnancy was induced
448 in the females by mating them with a vasectomized male. Prior to implantation, the pseudopregnant
449 females were anesthetized with ketamine (100 mg/kg) and xylazine (10 mg/kg) through intraperitoneal
450 injection, and the surgical embryo transfer procedure was performed following the protocol described
451 by Behringer et al. (Manipulating the Mouse Embryo, a Laboratory Manual, fourth edition, Chapter 6,
452 Richard Behringer et al. Cold Spring Harbor Laboratory Press, 2014). Postoperative analgesic treatment
453 with carprofen (5 mg/kg) was administered subcutaneously for 48 hours.
454
455 ***8-cell-morula blastomere disaggregation:***

456 miRNAs were injected in the embryo at zygote stage as described above. After injection, embryos were
457 incubated in KSOM (KSOM-Embryomax advanced embryo medium, Merck Millipore #MD-101-D)
458 for 48-56 hours at 37 °C, in 5% $C0_2$. The culture medium was refreshed daily. In the afternoon of the
459 third day of culture, when the embryos had reached the 8-cell morula stage, they were incubated at RT
460 in Tyrod's solution (Sigma-Aldrich T1788) for up to 30 seconds until the zona pellucida was completely
461 dissolved. Afterwards the naked morulas were washed through three drops of M2 medium (Sigma-
462 Aldrich M7167), and finally incubated in KSOM without Ca^{2+} and Mg^{2+} at RT for 20 minutes. Then,
463 embryos were moved to a new drop of fresh M2 medium and there, pipetted up and down repeatedly to
464 facilitate the blastomere disaggretation. When single blastomeres were obtained, they were individually
465 transferred to single wells of a 96-well single-cell-sequencing plate from VWR (Cat. No. 82006-636)
466 with 2 ul of RNAse inhibitor mix (containing 0.12 ul Triton X-100 10 %, 0.1 ul RNAse inhibitor (Takara
467 (Cat. No. 2313B, 40 U/ul), 1.78 ul MilliQ water (RNAse-free)). Plates were them frozen at -80 °C until
468 the sequencing was performed.
469
470 ***Lipodomics and Metabolomics:***
471 ***Serum Extraction:***
472 100 µL of serum was mixed with 1000 µL of a 2:1 chloroform/methanol solution and 200 µL of water.
473 Four blank samples, each containing 100 µL of water, were processed in parallel. The mixtures were
474 shaken at 1000 rpm for 30 minutes at 4°C, followed by centrifugation at 16,000g for 10 minutes at 4
475 °C to separate the phases. The aqueous phase was re-extracted with 350 µL of an 86:14:1
476 chloroform/methanol/water solution. The organic phase from this re-extraction was combined with the
477 corresponding organic phase from the initial extraction. Aqueous fraction was dried using SpeedVac,
478 while the organic phase was dried under a stream of nitrogen. For subsequent analysis, the dried aqueous
479 fractions were reconstituted in 30 µL of 1 % formic acid for metabolomics. The organic phase was
480 reconstituted in 30 µL of lipidomics solvent A (5:1:4 isopropanol/methanol/water with 5 mM
481 ammonium acetate and 0.1 % acetic acid). A pooled quality control sample was prepared for each
482 analytical setup by combining 5 µL from each sample, excluding blanks.
483

484 ***Lipidomic analysis:***

485 For lipidomics analysis, 2.5 µL of each sample was injected into an Agilent 1290 Infinity UPLC system
486 (Agilent Technologies, Santa Clara, CA, USA) equipped with a Zorbax Eclipse Plus C18 guard column
487 (2.1 × 5 mm, 1.8 µm) and an analytical column (2.1 × 150 mm, 1.8 µm), maintained at 50 °C. Analytes
488 were eluted at a flow rate of 400 µL/min using eluent A (water with 5 mM ammonium acetate and 0.1
489 % acetic acid) and eluent B (99:1 isopropanol/water with 5 mM ammonium acetate and 0.1 % acetic
490 acid). The gradient was as follows: 0 % B from 0 to 1 min, 0-25 % B from 1 to 1.5 min, 25-95 % B
491 from 1.5 to 12 min, 95 % B from 12 to 14 min, and 95-0 % B from 14 to 15 min, followed by a 3-
492 minute equilibration.

493 For metabolomics analysis, 1.5 µL of each sample was injected into the same UPLC-MS system, but
494 with a ZORBAX Eclipse Plus C18 guard column (2.1 × 50 mm, 1.8 µm) and an analytical column (2.1
495 × 150 mm, 1.8 µm) maintained at 40°C. Eluent A was 0.1 % formic acid, and eluent B was 0.1 % formic
496 acid in acetonitrile. The gradient was as follows: 3 % B from 0 to 1.5 min, 3-40 % B from 1.5 to 4.5
497 min, 40-95 % B from 4.5 to 7.5 min, 9 5% B from 7.5 to 10.1 min, and 95-3 % B from 10.1 to 10.5 min,
498 followed by a 3.5-minute equilibration.

499 Both analyses were performed on a 6530B quadrupole time-of-flight mass spectrometer (Agilent
500 Technologies, Santa Clara, CA, USA) for mass spectrometric detection in positive and negative ion
501 modes. MS1 mode settings included a scanning range of 50-1700 m/z for lipidomics and 10-1050 m/z
502 for metabolomics, with 2 scans/sec. Internal calibration was performed using Hexakis(1H,1H,3H-
503 tetrafluoropropoxy) phosphazene delivered through a second needle in the ion source via an isocratic
504 pump running at 20 µL/min. Iterative data-dependent MS2 mode was used for fragmentation in both
505 analyses with the following settings: collision energy at 40 V (lipidomics) and 20-40 V (metabolomics),
506 precursor threshold at 5000 counts, and active exclusion after 2 spectra, with re-inclusion after 0.5 min.

507

508 ***Data Processing and Normalization:***

509 All data was converted. mzML format using ProteoWizard[70]. Lipidomics data was annotated in MS-
510 Dial (v. 4.9) against the incorporated lipid-blast[71] with an MS1/MS2 mass tolerance of 0.005/0.01 Da
511 and a minimum identification score of 70 %. The annotated compounds were exported to PCDL

512 manager B.08.00 (Agilent Technologies) to create a database for area extraction in Profinder 10.0
513 (Agilent Technologies). Metabolomics data was processed in MzMine (v2.59) utilizing modules such
514 as ADAP chromatogram builder and deconvolution. Compounds were annotated at Metabolomics
515 Standards Initiative (MSI) levels 3 using the libraries of National Institute of Standards and Technology
516 2017 (NIST17) and MassBank of North America (MoNa). Features with signals less than 5 times those
517 in blanks or missing in more than 20 % of QC samples were removed and signals were QC corrected
518 using statTarget[72].
519
520 ***Serum insulin and leptin ELISA:***
521 Serum insulin and leptin levels were measured by mouse insulin ELISA kit (Mercodia, Uppsala,
522 Sweden) and mouse leptin ELISA kit (Crystal Chem, IL, USA) according to manufactures' protocol.
523
524 ***Histology and staining:***
525 Liver and adipose tissues fixed with 4 % of paraformaldehyde were used for histology analyses.
526 Formalin-fixed, paraffin-embedded tissues were cut into 3 µm sections. Sections were stained by
527 hematoxylin and eosin (H&E) and Sirius Red by standard procedures at the Department of Pathology
528 at Odense University Hospital, Odense, Denmark. Immunohistochemistry for CD45 was performed on
529 Ventana BenchMark Ultra (Roche) with ready-to-use CD45 (LCA) (2B11 & PD7/26) Mouse
530 Monoclonal Antibody. A liver pathologist (SD) assigned steatosis grades as S0 (< 5% hepatocytes with
531 large fat vacuoles), S1 (5-33%), S2 (>33-66%), and S3 (>66% hepatocytes with large fat vacuoles)[73].
532 Lobular inflammation (0-3) and hepatocellular ballooning (0-2) were assessed according to the NAS-
533 CRN Activity Score. In addition, portal inflammation was assessed, using a 4-tiered score. Liver fibrosis
534 stage was assessed according to NAS-CRN for fibrosis; F0, no fibrosis; F1, perisinusoidal or periportal
535 fibrosis; F2, perisinusoidal and portal/periportal fibrosis; F3, bridging fibrosis; F4, cirrhosis.
536
537 ***Measurement of adipocyte volumes:***

538 The volume weighted mean volume of adipocytes was determined from the H&E sections with
539 newCAST stereology software (Visiopharm), autodisector; measurements on systematic, randomly
540 selected fields were performed on by at least 75 adipocyte profiles in each tissue.
541
542 ***Bulk proteomics from epididymal white adipose tissue:***
543 Deep frozen fat pads (200 mg of epididymal adipose tissue) were powdered with mortar-pestle and
544 subjected to homogenization with ceramic beads (Percellys, 5500 rpm, 2 x 10 seconds, 30 seconds
545 break) in the buffer containing 50 mM HEPES pH 7.4, 1 % Triton X-100, 100 mM NaF, 10 mM sodium
546 orthovanadate, 10 mM EDTA, 0.2 % SDS, 100 mM NaCl. Tissue homogenates were further processed
547 to remove the nucleic acid traces (Diagenode SA; 10 min, cycle 30/30 seconds, at 4 °C). Floating fat
548 and tissue debris were removed from protein extracts by centrifugation at 20000 x g. 150 mg of proteins
549 were precipitated with 4x volume of ice-cold acetone and washed with ice-cold acetone twice. Air-dry
550 pellets were resuspended in 8M Urea/50 mM triethylammonium bicarbonate (TAEB) buffer
551 supplemented with a protease inhibitor cocktail (Sigma). 50 mg of the samples were incubated with 5
552 mM dithiothreitol at 25°C for 60 min, followed by treatment with 40 mM chloroacetamide for 30 min
553 (room temperature, light-protected). Lys-C protease (enzyme: substrate ratio of 1:75) was added for 4
554 hours at 25 °C. The TAEB-diluted sample (2M Urea final) was supplemented with trypsin (1:75 ratio)
555 followed by overnight digestion at 25 °C. Acidified peptides (1 % formic acid final) were purified on
556 the SDR-RP (C18) multi-stop-and-go-tip (Stage Tip)[74].
557
558 ***LC MS/MS Label-Free Quantitative Proteomic Analysis from epididymal white adipose tissue:***
559 All samples were analyzed by the Proteomics Facility on a Q Exactive Plus Orbitrap mass spectrometer
560 coupled to an EASY nLC 1000 (both Thermo Scientific). Peptides were loaded with solvent A (0.1 %
561 formic acid in water) onto an in-house packed analytical column (50 cm - 75 µm I.D., filled with 2.7
562 µm Poroshell EC120 C18, Agilent) and separated with 150 min gradients. Peptides were
563 chromatographically separated at a constant flow rate of 250 nL/min using the following gradient: 4-6
564 % solvent B (0.1 % formic acid in 80 % acetonitrile) within 5.0 min, 6-23 % solvent B within 120.0
565 min, 23-54 % solvent B within 7.0 min, 54-85 % solvent B within 6.0 min, followed by washing and

566 column equilibration. The mass spectrometer was operated in data-dependent acquisition mode. The
567 MS1 survey scan was acquired from 300-1750 m/z at a resolution of 70,000. The top 10 most abundant
568 peptides were isolated within a 2.1 Th window and subjected to HCD fragmentation at a normalized
569 collision energy of 27 %. The AGC target was set to 5E5 charges, allowing a maximum injection time
570 of 60 ms. Product ions were detected in the Orbitrap at a resolution of 17,500. Precursors were
571 dynamically excluded for 20.0 s. All mass spectrometric raw data were processed with MaxQuant[75]
572 (version 1.5.3.8, using default parameters and searched against the canonical murine Uniprot reference
573 proteome (UP589, downloaded on 28/08/2020). Label-free quantification option was enabled as was
574 the match-between runs option between replicates. Follow-up analysis was done in Perseus[76] 1.6.15.
575 Hits from the decoy database, the contaminant list, and those only identified by modified peptides were
576 removed. Afterwards, results were filtered for data completeness in replicate groups and LFQ values
577 imputed using sigma downshift with standard settings. Finally, FDR-controlled T-tests between sample
578 groups were performed with s0 = 0.2. Proteins were annotated on GOBP, GOCC, KEGG and Pfam
579 terms. Afterwards, all one-way ANOVA (s= 0.2) significant candidates were Zscored and hierarchically
580 clustered using the Euclidean distance model. Resulting clusters were merged onto the whole data set
581 and a Fisher Exact Test calculated on cluster level with the whole dataset as background.
582
583 ***RNA isolation from mouse tissue and primary adipocytes:***
584 Total RNAs from tissues, sperm, and primary adipocytes were isolated using the TRI reagent (Sigma)
585 followed by clean-up with RPE buffer (Qiagen, Germany). The quality of RNA was validated by the
586 Agilent RNA 6000 Nano-Kit in Agilent 2100 Bioanalyzer according to the manufacturer's protocol.
587 (Agilent Technologies, Waldbronn, Germany).
588
589 ***RNA sequencing:***
590 ***Small RNA sequencing:***
591 (1) For sRNA-seq from F_0 sperm, library preparation and sRNA-seq was performed at Cologne Center
592 for Genomics, Germany. 50 ng of total RNA was used for library preparation followed by size selection
593 (Small RNA-Seq Library Prep Kit, Lexogen). The library was sequenced in 1x50-bp single-end reads

594 on NovaSeq6000 serie no. A00316. (2) Small RNA sequencing from F_0 and F_1 eWAT was carried out
595 after quality control, 125 ng of total RNA was used for library preparation (Nextflex library kit)
596 followed by sequencing by 1x50-bp single-end reads on Illumina Novaseq 6000.
597
598 ***mRNA sequencing:***
599 mRNA sequencing was performed in-house. After quality control, 1 µg of total RNA was used for
600 library preparation (NEBNext RNA prep kit) followed by 2x50bp paired-end sequencing on Illumina
601 Novaseq 6000.
602
603 ***RNAseq data analysis:***
604 Sequencing reads were aligned to the mouse reference genome from Gencode (vM25)[77] using STAR
605 aligner (v 2.7.9a)[78] and gene features were counted by using featureCountsv (2.0.3)[79]. The genes with
606 low expression were filtered out using *filterByExpr* function with default settings (apart from "Embryo
607 Inject" dataset, where parameter min.count was set to 40 as more rigorous filtering was required) from
608 edgeR (v4.0.16)[80] R package. Differential expression analyses were performed using edgeR's
609 *voomLmFit* [81]unction with sample quality weights (sample.weights = TRUE) and linear model "0 +
610 group", whereas group represents the combination of all experimental groups of interest. The
611 experimental conditions and linear models used for each dataset are summarized below. Genes with
612 adjusted p-values below 0.05 were considered as differentially expressed. Gene enrichment analyses
613 were performed by clusterProfiler (v4.10.1)[82] R package using both over-representation analysis (ORA)
614 and gene-set enrichment analysis (GSEA) using differentially expressed genes and log-fold-change
615 (logFC) ranked genes ($n_{permutation}$ = 1,000,000), respectively. Gene sets were retrieved from Gene
616 Ontology (GO.db v3.18.0) and Reactome (reactome.db, v1.86.2) databases.
617
618 ***Smart-seq2 mRNA sequencing of murine blastomeres:***
619 Custom-made Smart-seq2 protocol was implemented as before[65]. Briefly, after thawing the plate, 1 µL
620 of dNTP mix (10 mM), 0.1 µL of oligo-dT (100 µM,
621 /5Biosg/AAGCAGTGGTATCAACGCAGAGTAC(T)30VN-3′) and 0.9 ul nuclease-free water was

added to each well and the lysis protocol was run when the samples were incubated at 72°C for 3 min in thermocycler. Samples were then put on ice for at least 1 min. Next, 5.60 µL of reverse-transcription mix containing 0.25 µL of RNase I, 2 µL of 5× first-strand buffer, 2 µL of betaine (5 M), 0.06 µL of $MgCl_2$ (1 M), 0.5 µL of DTT (100 mM), 0.5 µL of SuperScript III (200 U/µL), and 0,29 ul of nuclease-free water was added to each well and reverse transcription was carried out as follows: 42 °C-90:00, 42 °C-hold, 42 °C—12:20, 10 cycles (50 °C-2:00, 42 °C-2:00), 39 °C-12:00, 70 °C-15:00, 4 °C hold. After the first 90 min of RT, 0.4 µL of 12,5 µM TSO (0.83 µM final concentration) was added to each reaction at room temperature. The plate was resealed, centrifuged for 1 min at 700 g, and placed back on the thermocycler to resume cycling from 42 °C-12:20. After reverse transcription, 15 µL of cDNA enrichment PCR reaction mix containing 12.5 µL of 2× KAPA HiFi HotStart ReadyMix, 0.25 µL of ISPCR primer (10 µM, /5Biosg/AAGCAGTGGTATCAACGCAGAGT-3′), and 2.25 µL of nuclease-free water was added to each well and cDNA enrichment PCR was performed as follows for 21 cycles: 98 °C-3:00, 7 cycles (98 °C-0:20, 60 °C-4:00, and 72 °C-6:00), 7 cycles (98 °C-0:20, 64 °C-0:30, and 72 °C-6:00), and 7 cycles (98 °C-0:20, 67 °C-0:30, and 72 °C-7:00), 72 °C-10:00, 4 °C-hold. The cDNA purification was performed using AMPure XP beads at a ratio of 1:1 (Beckmann). For elution, Qiagen elution buffer (EB) was used. cDNA concentrations were measured using the Qubit 3.0 fluorometer according to the manufacturer's protocol, and all cDNA samples were analyzed on Agilent Tape station using the High Sensitivity DNA assay.

Dual-indexed Illumina Nextera XT sequencing libraries were prepared using 25 % of the recommended reaction volumes of Nextera XT components. All Nextera XT libraries were prepared using 125 pg of input cDNA for tagmentation, and were subsequently enriched for 12 PCR cycles, and purified using AMPure XP beads (Beckmann) at a sample:bead ratio of 0.6:1. Library concentrations were measured using Qubit 3.0 fluorometer, and the fragments were analyzed on the Agilent Tape station using the High Sensitivity DNA assay. All libraries were individually normalized and diluted to a concentration of pooled library to 5.4 ng/µL with average size ~515bp (16 nM). The libraries were sequenced on Illumina NextSeq500 in a single-end 75-bp format (FC-404-2005, Illumina). Single-nuclei libraries were sequenced at an average depth of 3 mio reads.

650

651 ***Data availability – NGS:***

652 (1) Illumina datasets (sRNA-seq, mRNA-seq) from F_0 / F_1 liver and eWAT are available as Gene
653 Expression Omnibus series under accession number [GEOxxx].

654 (2) Illumina datasets (sRNA-seq) from F_0 sperm are available as Gene Expression Omnibus series
655 under accession number [GEOxxx].

656 (3) Illumina datasets (mRNA-seq) from offsprings of miRNA-injected zygotes (F_m) eWAT are
657 available as Gene Expression Omnibus series under accession number [GEOxxx].

658 (4) Illumina datasets (mRNA) from 1°eWA overexpressing Negative Control, *miR-let-7d-5p, miR-let-*
659 *7e-5p* mimics are available as Gene Expression Omnibus series under accession number
660 [GEOxxx].

661 (5) Smart-Seq2 single-cell mRNA-seqdata from miRNA-injected 8-cell stage embryos are available
662 as Gene Expression Omnibus series under accession number [GEOxxx]

663

664 ***Data availability – Proteomics:***

665 The mass spectrometry proteomics data have been deposited to the ProteomeXchange Consortium via
666 the PRIDE [1] partner repository with the dataset identifier PXD042800. The data are available to the
667 reviewer discretion: **Username:** reviewer_pxd042800@ebi.ac.uk**, Password:** QHj9fv33

668

669 ***Data availability – Metabolomics:***

670 []

671

672 ***Male participants, sperm samples and analysis***

673 The intervention study was approved by the Danish National Committee on Health Research Ethics
674 (SJ-769), the Danish Data Protection Agency (REG-048- 2019) and performed at the Fertility Clinic,
675 Zealand University Hospital, Denmark[62]. The semen samples were collected from obese patients
676 (≥ 30 kg/m2) via masturbation following two days of abstinence. The sperm analyses were performed
677 in the IVF laboratory in an authorized tissue establishment. The other semen samples were diluted with

678 MHM-C (Fujifilm) and frozen immediately for further analysis. The semen samples were collected via
679 masturbation following two days of abstinence, and the samples were analyzed a maximum of two to
680 three hours after production. After liquefaction, ejaculate volume and sperm concentration (total, motile
681 and progressive) were assessed using a microscope (Leica DM750). Sperm concentration was
682 determined with a CellVision counting chamber (CellVision Technology, Heerhugowaard, the
683 Netherlands). Total sperm count was calculated as the product between ejaculate volume and sperm
684 concentration. The sperm analyses were performed in the IVF laboratory in an authorized tissue
685 establishment.
686
687 ***Study design and approvals***
688 This prospective intervention study was conducted between May 2020 and April 2022 at the Fertility
689 Clinic, Zealand University Hospital, Denmark. The study was approved by the Danish National
690 Committee on Health Research Ethics (SJ-769), the Danish Data Protection Agency (REG-048- 2019)
691 and registered on the Clinical Trial website (www. ClinicalTrials.gov identifier NCT04721938). All
692 participants provided written informed consent.
693
694 ***Primary adipocyte culture and transfection***
695 Epididymal white adipose tissues (eWAT) from 6- to 8-week-old male C57BL/6J mice were removed,
696 minced, and digested with pre-warmed collagenase media (500 U/mL collagenase type 2 (LS004183,
697 Worthington) and 3.75U/mL DNase I (10104159001, Sigma). Isolated cells were seeded in 6-well
698 plates and grown in DMEM/Ham's F12 medium (21331, Vendor: Gibco), supplemented with 0.1 %
699 Biotin/D-Pantothenate (33 mM/17 mM), 1 % penicillin-streptomycin, and 20 % FBS. Until reaching
700 80 % confluency, primary cells were induced by induction medium with 1 μM rosiglitazone, 850 nM
701 insulin, 1 μM dexamethasone, 250 μM 3-isobutyl-1-methyl-xanthin (IBMX) and 10 % FBS.
702 Subsequently, the medium was changed every other day by a differentiation medium containing 1 μM
703 rosiglitazone, 850 nM insulin and 10 % FBS. 100 nM of Negative Control and *mmu-miR-let-7-d/e-5p*
704 mimics or LNA oligos tageting *Dicer1* were reversely transfected using Lipofectamine RNAiMAX

705 (Thermo Fisher Scientific) at day 4 after induction. Completely differentiated cells were harvested at 7
706 days after induction for further analysis.
707
708 ***Plasmid design and dual luciferase assay***
709 For the generation of reporter constructs, the specific region of murine *Ago2*, *Dicer-1*, *Hif1an*, *Hk2*,
710 *Cpt2*, *Crat*, *Pcx*, *Idh2*, *Sdha*, *Sdhaf3*, *Pdk2*, *Slc25a22* and *Slc25a24* containing either the wildtype (wt)
711 or mutated (mut) *miR-let-7* binding sites was cloned behind the translation stop codon of the firefly-
712 luciferase gene in pmirGLO Dual-Luciferase vector using custom DNA oligos provided by IDT. Renilla
713 luciferase coding in the same plasmid was used as a control reporter for normalization purposes. To
714 report the miRNA activity in mammalian cells, HEK 293 cells were reversely transfected in 96-well
715 plates with 60 ng DNA using the TransIT transfection reagent (mirusbio) for 3 days and forwardly
716 transfected with *miR-let-7d/e-5p* mimics for 2 days. HEK-293 cells were cultured in DMEM medium
717 (21013, Gibco) supplemented with 5.6 mM L-glutamine, 1 % penicillin-streptomycin, and 10 % FBS.
718 After 72-h vector transfection and 48-h miRNA mimics transfection, dual luciferase reporter assays
719 (Promega) were performed. The relative activities of firefly luciferase indicating the interaction
720 between miRNA and specific region of targeted mRNA were normalized by the activities of Renilla
721 luciferase.
722
723 ***TaqMan assay and general qPCR***
724 To quantify the levels of mature miRNAs, TaqMan MicroRNA Reverse Transcription Kit (4366596,
725 Thermo Fisher), TaqMan MicroRNA Assays and TaqMan Universal Master Mix II (4440042, Thermo
726 Fisher) were applied according to manufacturer's protocols. Level of mature *hsa-miR-16* was used as
727 internal control in human samples. The relative expression of mature miRNA was calculated using a
728 comparative method (2- ∂∂CT) according to the ABI Relative Quantification Method.
729
730 ***Determination of oxygen consumption rates and measurement of glycolytic activity:***
731 Primary adipocytes from epididymal SVF (1°eWA) were seeded into Agilent Seahorse XFe96
732 Bioanalyzer microplates. Induction and differentiation were performed as described above. After four

733 days of differentiation, 16,000 per well mature adipocytes were re-seeded and transfected with LNA
734 oligos targeting *Dicer1* in DMEM/Ham's F-12 medium plus 10 % Fetal Bovine Serum, 1 % P/S, 0.1 %
735 Biotin and 0.1 % Pantothenic acid (Growth medium) at 37° C and 5 % CO_2. Seahorse measurement
736 was conducted at day 7 from differentiation. For each seahorse plate, the corresponding calibration plate
737 was prepared 24 hours prior to experiments using 200 µl XF Seahorse Calibrant Agilent per well.
738 Corresponding media were prepared before the experiment and consisted of Assay Medium
739 supplemented with 25 mM Glucose, 1 mM Glutamine, 2 mM Sodium Pyruvate, set to pH = 7.4 and
740 filtered sterile. The calibration plate possessed a cartridge having 4 pockets per well. Shortly before the
741 measurement pocket A was filled with 20 µl 20 µM Oligomycin, pocket B with 22 µl 20 µM FCCP and
742 pocket C with 25 µl 5 µM Antimycin A and Rotenone. One hour before measurements, plates were
743 washed with 1x PBS and changed to 180 µl Assay Medium in a non-CO_2 incubator at 37° C. Calibration
744 was started using calibration plates, measuring O_2 and pH LED Value/emission/Initial reference Delta
745 for each well. All measurements started with measuring basal values, followed by injection of
746 Oligomycin, FCCP, and Rotenone plus Antimycin A (MitoStressKit). Measurement parameters were:
747 Mix 3 min, wait 0 min, measure 3 min with each reagent's effect assessed within three consecutive
748 measurement cycles with a total duration of 18 min per reagent injection.
749
750 ***Protein extraction and western blot analysis***
751 After being washed once by phosphate-buffered saline (PBS), the treated cells at harvest time were
752 lysed by RIPA buffer supplemented with cOmplete and PhosSTOP and quantified by Pierce BCA
753 Protein Assay Kit (23227, Thermo Fisher). Western blot analyses were carried out according to standard
754 protocols with primary antibodies listed in **Table S1**. Relative protein quantification was normalized
755 by HSC70.
756
757 ***Statistical analysis***
758 Data were shown as mean ± standard error. One-way ANOVA and two-way ANOVA followed by
759 Tukey's multiple comparisons test were used for statistical analysis in *in vivo* experiments. Significant
760 differences between groups were noted in figure legends respectively.

Acknowledgements:

We thank the CECAD Proteomics Core Facility for support with proteomics analyses, the Laboratory Manager, Stine Ravn, at The Zeland Fertility Clinic for handling and analyzing the sperm samples. We wish to thank Bente Møller and Irina Korshuniova from BRIC Single Cell Genomics Core Facility for excellent help for Smart-seq2 experiments. Smart-seq2 work was partly supported by CellX (The Danish Single Cell Examination Platform) funded by the Danish Research Agency through the Danish national research infrastructure program (5229-0009B). JWK, JHP and BDML received funding from the European Research Council Starting Grant TransGenRNA (#675014), JWK, CH and NS from Sygeforsikring Denmark, University of Southern Denmark and the Danish Diabetes Academy (DDA), which is funded by the Novo Nordisk Foundation (NNF17SA0031406). JWK received support from the NNF Challenge (33444) and Bioscience and Basic Biomedicine Programs of the NNF (28416).

773 **Figure legends**

774

775 **Figure 1: Obesity and weight loss elicit reversible changes in glucose metabolism and**
776 **mitochondrial metabolites.** (**a**) Illustration of intergenerational *in vivo* cohorts depicting F_0 groups of
777 obese and weight-regression C57BL/6N male mice, F_1 offsprings and the overall analytical workflow.
778 (**b**) Body weights of F_0 LF (n=6), F_0 HF (n=13; n=6 for 15-24 weeks of age,), F_0 HF-LF (n=7). (**c,d**)
779 Blood glucose levels (**c**) and area under the curve (AUC) of glucose levels in (**d**) during intraperitoneal
780 glucose tolerance test (ipGTT) in F_0 LF (n=6), F_0 HF (n=6) and F_0 HF-LF (n=7) mice. (**e**) Relative blood
781 glucose levels during intraperitoneal insulin tolerance test (ipITT) in F_0 LF (n=6), F_0 HF (n=6) and F_0
782 HF-LF (n=7) mice. (**f**) Random-fed blood glucose in F_0 LF (n=6), F_0 HF (n=6) and F_0 HF-LF (n=7)
783 mice. (**g**) Serum insulin levels as measured by ELISA in F_0 LF (n=6), F_0 HF (n=6) and F_0 HF-LF (n=7)
784 mice. (**h**) Serum leptin levels measured by ELISA in F_0 LF (n=6), F_0 HF (n=6) and F_0 HF-LF (n=7)
785 mice. (**i**) Relative organ weights in F_0 LF (n=6), F_0 HF (n=6) and F_0 HF-LF (n=7) mice. (**j**) Illustration
786 of organ acquisition and multi-modal omic methodologies (**k**) Principal component analysis (PCA) and
787 PC1-3 representation of n=600 polar metabolites in serum of F_0 LF (n=6), F_0 HF (n=6) and F_0 HF-LF
788 (n=7) mice. (**l**) Correlation cofficients and ID of serum metabolites irreversibly (*left*, n=95) or reversibly
789 (*right*, n=118) altered in F_0 HF/F_0 HF-LF vs F_0 LF mice. Data in (**k,l**) were analyzed and plotted using
790 Metaboanalyst 6.0 (https://www.metaboanalyst.ca/MetaboAnalyst/). (**m**) Illustration of differential
791 metabolite abundances from (**k,l**) in the tricarbon acid cycle (TCA) pathway in serum of F_0 LF (n=6),
792 F_0 HF (n=6) and F_0 HF-LF (n=7) mice. One-way ANOVA (**d**,**f-i**) and two-way ANOVA (**b**,**c**,**e**) followed
793 by Tukey's multiple comparisons test were used for statistical analysis. Data are presented as mean ±
794 standard error (**b,c,e**) or individual values and superscript letters represent group comparisions (**a**,
795 $p<0.05$, F_0 LF vs F_0 HF; **b**, $p<0.05$, F_0 LF vs F_0 HF-LF; **c**, $p<0.05$, F_0 HF vs F_0 HF-LF).

796

797 **Figure 2. Multimodal omics analysis reveals reversible mitochondrial gene aberrations in obese**
798 **adipose tissue.** (**a**) Representative hematoxylin and eosin (H&E) stainings in eWAT of F_0 LF, F_0 HF
799 and F_0 HF-LF mice. (**b**) Size distribution of adipocytes area in eWAT of F_0 LF (n=6), F_0 HF (n=6) and
800 F_0 HF-LF (n=6) mice. (**c**) Multidimensional scaling (MDS) plots of transcriptomic changes in eWAT

801 as determined by m RNA-seq. Dots represent eWAT from individual animals, n=6 per group. (**d-g**)
802 Volcano plot of significantly up-(red) and down-regulated (blue) differentially expressed genes (DEG)
803 in eWAT from (**d**) F_0 HF vs F_0 LF, 3,867 upregulated and 2,337 downregulated DEG, (**e**) F_0 HF vs F_0
804 HF-LF, 2,858 upregulated and 1,986 downregulated DEG and (**f**) F_0 HF-LF vs F_0 LF, 459 upregulated
805 and 262 downregulated DEG. Plots depict log2 transformed fold-changes and log10- transformed false-
806 discovery rates (FDR) of expression changes. Significant DEG are defined as FDR≤0.05. (**g**) Gene Set
807 Enrichment Analysis (GSEA) and gene ontology (GO) enrichment of biological processes (GOBP) of
808 DEG shown in (**d-f**). (**h**) Heatmap depicting relative abundances of miRNAs in F_0 LF (n=6), F_0 HF
809 (n=6) and F_0 HF-LF (n=6) eWAT as determined by small RNA-seq. Boxes depict miRNAs that were
810 reported to positively (*brown*) or negatively (*red*) affect mitochondrial biogenesis and function. (**i**)
811 Abundance of positive (*miR-143-3p*, *miR-181a-2-3p*, *miR-378a-3p* and *miR-378*, brown) and negative
812 (*miR-532-5p*, red) miRNA regulators in F_0 LF (n=6), F_0 HF (n=6) and F_0 HF-LF (n=6) eWAT. One way
813 ANOVA (**b,i**) followed by Tukey's multiple comparisons test were used for statistical analysis. Data
814 are presented as individual values and superscript letters represent group comparisions (**a**, $p<0.05$, F_0
815 LF vs F_0 HF; **b**, $p<0.05$, F_0 LF vs F_0 HF-LF; **c**, $p<0.05$, F_0 HF vs F_0 HF-LF). (**j**) Schematic representation
816 of miRNA-mRNA differential expression networks using Cytoscape (https://cytoscape.org/). Shown
817 are predicted mRNA targets of miRNA from (**i**) as identified by AGO-HITS-CLIP in adipose tissue
818 from[56]. Node color depicts differential expression of predicted miRNA targets (F_0 HF (n=6) vs F_0 LF
819 (n=6)) and yellow highlights miRNA seed lengths (*left*, 7mer; *right*, 8mer). Edge color depits genic
820 localisation of the lontest miRNA seed.
821
822 **Figure 3: Paternal obesity impairs glucose tolerance and instigates adipose dysfunction in F1**
823 **adipose tissue.** (**a**) Body weight of F_1 [F_0 LF] (n=18), F_1 [F_0 HF] (n=25) and F_1 [F_0 HF-LF] (n=21). (**b,c**)
824 Blood glucose levels (**c**) and AUC of glucose levels during IPGTT in F_1 [F_0 LF] n=10), F_1 [F_0 HF]
825 (n=10) and F_1 [F_0 HF-LF] (n=10) mice. (**d**) Relative blood glucose levels during IPITT in F_1 [F_0 LF]
826 (n=10), F_1 [F_0 HF] (n=10) and F_1 [F_0 HF-LF] (n=9) mice. (**e**) Random-fed serum glucose levels in F_1
827 [F_0 LF] (n=18), F_1 [F_0 HF] (n=25) and F_1 [F_0 HF-LF] (n=21) mice. (**f**) Serum insulin levels measured by
828 ELISA in F_1 [F_0 LF] (n=6), F_1 [F_0 HF] (n=8) and F_1 [F_0 HF-LF] (n=8) mice. (**g**) Serum leptin levels

829 measured by ELISA in F_1 [F_0 LF] (n=7), F_1 [F_0 HF] (n=8), and F_1 of F_0 HF-LF (n=8) mice. (**h**) Body
830 composition measured by DXA in F_1 [F_0 LF] (n=11), F_1 [F_0 HF] (n=11) and F_1 [F_0 HF-LF] (n=11) mice.
831 (**i**) relative organ weights of F_1 [F_0 LF] (n=10), F_1 [F_0 HF] (n=10) and F_1 [F_0 HF-LF] (n=7). (**j,k**)
832 Representative H&E staining (**j**) and size distribution (**k**) of adipocytes in eWAT of F_1 [F_0 LF] (n=6),
833 F_1 [F_0 HF] (n=6) and F_1 [F_0 HF-LF] (n=6) mice. (**l**) GSEA-GOBP analysis of DEGs in eWAT of F_1 [F_0
834 LF] (n=4) F_1 [F_0 HF] (n=6) and F_1 [F_0 HF-LF] (n=6) mice. (**m,n**) Heat map and hierarchical clustering
835 differentially translated genes (**m**) and relative protein abundances (LFQ) of NDUFA6 and COX6B1
836 in eWAT of F_0 LF (n=6), F_0 HF (n=6), F_0 HF-LF (n=6), F_1 [F_0 LF] (n=6), F_1 [F_0 HF] (n=6), and F_1 of F_0
837 REV (n=6). One-way ANOVA (**c,g,i, k,n**) and two-way ANOVA (**b**) followed by Tukey's multiple
838 comparisons test were used for statistical analysis. Data are presented as mean ± standard error (**b,d**) or
839 individual values and superscript letters represent group comparisions (**a**, $p<0.05$, F_0 LF vs F_0 HF; **b**,
840 $p<0.05$, F_0 LF vs F_0 HF-LF; **c**, $p<0.05$, F_0 HF vs F_0 HF-LF).
841
842 **Figure 4: Obesity induces spermatozoa and adipose miR-let-7 and blunts adipocyte mitochondrial**
843 **function via a miR-let-7-DICER1 axis.** (**a,b**) Heatmap (**a**) and log10-transformed counts (**b**) of *miR-*
844 *let7* isoforms in sperm from F_0 LF (n=6), F_0 HF (n=6) and F_0 HF-LF (n=6) mice. One-way ANOVA
845 followed by Tukey's multiple comparisons test was used for statistical analysis. Superscript letters
846 represent group comparisions and P values are indicated in the panel. (**c**) Heatmap representation of
847 shown *miR-let-7* isoforms in F_0 LF (n=5), F_0 HF (n=5), F_0 HF-LF (n=5), F_1 [F_0 LF] (n=6), F_1 [F_0 HF]
848 (n=5), and F_1 of F_0 REV (n=5) eWAT and spermatozoa. (**d**) Illustration of experimental workflow and
849 methodology to characterize the effects of *miR-Let-7d-5p* and *miR-Let-7e-5p* in 1°eWA from
850 C57BL/6N mice. (**e**) Absolute expression (Cq value) of *miR-let7-d-5p* and *miR-let7-e-5p* in 1°eWA
851 transfected with 100nM Negative Control, *miR-let7-d-5p* and *miR-let-7e-5p*. (**f,g**) Volcano plot of
852 significantly up- (red) and down-regulated (blue) DEG in 1°eWA transfected with 100nM of (**f**) *miR-*
853 *let7-d-5p* vs Negative Control, 1,301 upregulated and 977 downregulated DEGs (**g**) *miR-let7-e-5p* vs
854 Negative Control, 635 upregulated and 759 downregulated DEGs. (**h**) Schematic representation of *miR-*
855 *let-7*-mRNA DEN, depicted predicted *miR-Let-7* target mRNA repressed in F_0 HF (n=6) vs F_0 LF (n=6)
856 with seed lengths ≥7nt using adipose tissue AGO-HITS-CLIP[56]. Node color depicts differential

857 expression of *miR-let-7* gene targets and yellow highlights genes from Mitocarta3.0 [69]. Edge color
858 depits the genic localisation of the *miR-Let-7* seed. (**i,j**) Relative luciferase activity in HEK293 cells
859 after co-transfection of pmirGLO dual luciferase reporter assay (DLRA) constructs harbouring (**i**) wild-
860 type 3′-UTR fragments of indicated genes or (**j**) wild-type and mutated fragments of *Dicer1*, *Hif1an*,
861 *Hk2* and *Slc25a24* transfected with 100nM of Negative Control, *miR-let-7d-5p* and *miR-let-7d-5p*
862 mimics. Data represent at least three biological replicates, each performed in three technical replicates.
863 One-way ANOVA (**j,k**) followed by Tukey's multiple comparisons test were used for statistical
864 analysis. Superscript letters represent group comparisions (**a**, $p<0.05$, Negative Control vs *miR-let-7d-*
865 *5p*; **b**, $p<0.05$, *miR-let-7e-5p* vs *miR-let-7e-5p*; **c**, $p<0.05$, Negative Control vs *miR-let-7e-5p*). (**k**)
866 Western blot analysis of 1°eWA transfected with 100nM of Negative Control, *miR-let-7d-5p* and *miR-*
867 *let-7d-5p* mimics performed with indicated antibodies. HSC70 served as loading control. (**l,m)** Oxygen
868 consumption rates (**l,** OCR) and extracellular acidification rates (**m**, ECAR) in 1°eWA transfected with
869 100nM of Negative Control A, *Dicer1* LNA1 and *Dicer1* LNA2 and stimulated with oligomycin (O),
870 FCCP (F) and Antimycin A plus Rotenone (A/R). Unpaired, two-tailed Student's t-tests were performed
871 at indicated timepoints (**a**, $p<0.05$, Negative Control vs *Dicer1* LNA1; **b**, $p<0.05$, *Dicer1* LNA1 vs
872 *Dicer1* LNA2; **c**, $p<0.05$, Negative Control vs *Dicer1* LNA2).
873
874 **Figure 5: Zygotic microinjection of obesity-associated *miR-let-7* causes F_1 glucose intolerance.**
875 (**a**) llustration of experimental workflow for zygotic miRNA injection and phenotypic characterisation
876 of sired offsprings (F_m mice). (**b**) Body weights of male F_m mice sired from zygotes injected with
877 Negative Control (n=9), *miR-let-7d-5p* (n=14), *miR-let-7e-5p* (n=14) and *miR-699-5p* (n=12). (**c-e**),
878 Organ weights of eWAT (**c**) and liver (**d**) from male F_m mice sired from Negative Control (n=7), *miR-*
879 *let-7d-5p* (n=6), *miR-let-7e-5p* (n=6) and *miR-699-5p* (n=7) treated zygotes. (**e**) Random-fed blood
880 glucose at indicated weeks of age in male F_m mice sired from Negative Control (n=7), *miR-let-7d-5p*
881 (n=6), *miR-let-7e-5p* (n=6) and *miR-699-5p* (n=7) treated zygotes. One way ANOVA followed by
882 Tukey's multiple comparisons test were used for statistical analysis. Data are presented as mean ±
883 standard error. **, $p<0.01$, Negative Control vs *miR-let-7d-5p*, *miR-let-7e-5p* and *miR-699-5p*. (**f-h**),
884 Blood glucose levels during IPGTT in male F_m mice sired from Negative Control (n=9), *miR-let-7d-5p*

885 (n=9), *miR-let-7e-5p* (n=9) and *miR-699-5p* (n=8) treated zygotes. Unpaired, two-tailed Student's t-
886 tests were performed at indicated timepoints and P values are indicated. (**i**) GSEA-GOBP analysis of
887 DEGs in eWAT of male F_m mice sired from Negative Control (n=5), *miR-let-7d-5p* (n=6) and *miR-let-*
888 *7e-5p* (n=6) treated zygotes.
889
890 **Figure 6: Obesity-associated *miR-let-7* rewires mitochondrial metabolism during embryogenesis.**
891 **(a,b**) Correlation plot and regression analysis between differential BMI changes (ΔBMI) and expression
892 changes in human semen *MIR-LET-7D-5P* (**a**) and *MIR-LET-7E-5P* (**b**). (**c**) Illustration of experimental
893 and analytical workflow to study differential mRNA expression in 8-cell blastomeres obtained from
894 Negative Control, *miR-let-7d-5p*, *miR-let-7e-5p*and *miR-699-5p* injected zygotes. (**d**) Multidimensional
895 scaling (MDS) of single-cell RNAseq profiles in 8-cell stage blastomeres obtained from Negative
896 Control (n=22), *miR-let-7d-5p* (n=19), *miR-let-7e-5p* (n=20) and *miR-699-5p* (n=21) injected zygotes.
897 (**e)** GSEA-GOBP analysis of DEGs depicted in (**d**).
898

899 **Supplementary figure legends:**

900

901 **Figure S1: Obesity and weight loss elicit reversible changes in serum metabolites associated with**
902 **mitochondrial function.**

903 **(a,b)** Relative abundances of TCA intermediate metabolites (**a**) and carnithin moities(**b**) as quantified
904 by LC-MS in serum of F_0 LF (n=6), F_0 HF (n=6) and F_0 HF-LF (n=7) mice. One-way ANOVA followed
905 by Tukey's multiple comparisons test were used for statistical analysis. P vales are indicated in each
906 panel.

907

908 **Figure S2: Obesity and weight loss elicits reversible induces serum lipids linked to mitochondrial**
909 **dysfunction.**

910 (**a,b**) Principal component analysis and PC1-2 representation (**a**) and heatmap illustration (**b**) of n=118
911 serum lipids from F_0 LF (n=6), F_0 HF (n=6) and F_0 HF-LF (n=7) mice. (**a,b)** were analyzed and plotted
912 using Metaboanalyst 6.0. (**c**) Relative abundances of ceramides species in serum of F_0 LF (n=6), F_0 HF
913 (n=6) and F_0 HF-LF (n=7) mice. One-way ANOVA followed by Tukey's multiple comparisons test
914 were used for statistical analysis and P vales are indicated in each panel.

915

916 **Figure S3: Paternal obesity and weight loss cause irreversible gene alterations in F_0 liver.**

917 (**a**) Representative histological (H&E), pan-leukocyte (anti-CD45) and anti-collagen/fibrosis (Sirius
918 Red) staining in livers of F_0 LF, F_0 HF and F_0 HF-LF mice. (**b-e**) Pathologist (SD) assessment of
919 macrovesicular (**b**) and microvesicular (**c**) steatosis (**d**) fibrosis and (**e**) lobular inflammation scores in
920 livers of F_0 LF (n=6), F_0 HF (n=6) and F_0 HF-LF (n=6) mice. A non-parametric Kruskal-Wallis test
921 followed by Dunn's multiple comparision test were used for statistical analysis and P vales are indicated
922 in each panel. (**f**) Multidimensional scaling (MDS) plot of F_0 liver. (**g-i**) Volcano plot of significantly
923 up-(red) and down-regulated (blue) differentially expressed genes (DEG) in liver from (**g**) F_0 HF vs F_0
924 LF, 3,495 upregulated and 1,639 downregulated DEG, (**h**) F_0 HF vs F_0 HF-LF, 2,858 upregulated and
925 1,986 downregulated DEG and (**i**) F_0 HF-LF vs F_0 LF, 459 upregulated and 262 downregulated DEG.
926 Plots depict log2 transformed fold-changes and log10- transformed false-discovery rates (FDR) of

927 expression changes. Significant DEG are defined as FDR≤0.05. (**j**) Gene Set Enrichment Analysis
928 (GSEA) and gene ontology (GO) enrichment of biological processes (GOBP) of DEG shown in (**g-i**).
929
930 **Figure S4: Reversible mitochondrial alterations in obese F_0 adipose tissue.**
931 (**a**) Multidimensional scaling (MDS) plots of transcriptomic changes in F_0 eWAT as determined by
932 RNA-seq. Dots represent eWAT from individual animals, n=6 per group. (**b**) Representation and colour
933 coding of mitochondrial electron transport chain complexes I-V (CI-V, *top*) and log-10 transformed
934 expression changes and significance of DEG (*bottom*) per CI-V in adipose tissue in eWAT of F_0 LF
935 (n=6), F_0 HF (n=6) and F_0 HF-LF (n=6) mice.
936
937 **Figure S5: Reversible mitochondrial alterations in obese F_1 adipose tissue.**
938 (**a**) Multidimensional scaling (MDS) plots of transcriptomic changes in F_1 eWAT as determined by
939 RNA-seq. Dots represent eWAT from F_1 [F_0 LF] (n=4), F_1 [F_0 HF] (n=6) and F_1 [F_0 HF-LF] (n=6) mice.
940 (**b**) Log-10 transformed expression changes and significance of DEG (*bottom*) per CI-V in adipose
941 tissue of eWAT of from F_1 [F_0 LF] (n=4), F_1 [F_0 HF] (n=6) and F_1 [F_0 HF-LF] (n=6) mice. (**c**) Relative
942 protein abundances (LFQ) of NDUFA8, NDUFS6, CPT1A and TOMM20 in eWAT of F_0 LF (n=6), F_0
943 HF (n=6), F_0 HF-LF (n=6), F_1 [F_0 LF] (n=6), F_1 [F_0 HF] (n=6), and F_1 of F_0 REV (n=6). One-way
944 ANOVA followed by Tukey's multiple comparisons test were used for statistical analysis. Data are
945 presented as mean ± standard error and P vales are indicated in each panel.
946
947 **Figure S6: Paternal obesity and weight loss cause irreversible gene alterations in F_1 liver.**
948 (**a**) Representative histological (H&E), pan-leukocyte (anti-CD45) and anti-collagen/fibrosis (Sirius
949 Red) staining in livers of F_1 [F_0 LF], F_1 [F_0 HF]and F_1 [F_0 HF-LF] mice. (**b-e**) Pathologist assessment of
950 macrovesicular (**b**) and microvesicular (**c**) steatosis, (**d**) lobular inflammation and (**e**) fibrosis scores in
951 livers of livers of F_1 [F_0 LF] (n=6), F_1 [F_0 HF] (n=6) and F_1 [F_0 HF-LF] (n=6) mice. A non-parametric
952 Kruskal-Wallis test followed by Dunn's multiple comparision test were used for statistical analysis and
953 P vales are indicated in each panel. (**f**) Multidimensional scaling (MDS) plot of F_1 liver. (**g-i**) Volcano
954 plot of up-(red) and down-regulated (blue) genes DEG in liver from (**g**) F_1 [F_0 HF] vs F_1 [F_0 LF] (**h**) F_1

955 [F_0 HF] vs F_1 [F_0 HF-LF] and (**i**) F_1 [F_0 HF-LF] vs F_1 [F_0 LF]. Plots depict log2 transformed fold-changes
956 and log10- transformed false-discovery rates (FDR) of expression changes. (**j**) Gene Set Enrichment
957 Analysis (GSEA) and gene ontology (GO) enrichment of biological processes (GOBP) of DEG shown
958 in (**g-i**).
959
960 **Figure S7: Reversible alterations in F_1 adipose mitochondrial proteins and identification of cross-**
961 **generational miRNAs.**
962 (**a**) Dot plot of enriched gene ontology terms in clusters I-III depicted of protein heatmap in **Fig.3m**.
963 (**b**) Heatmap depicting relative abundances of miRNAs in eWAT of F_1 [F_0 LF], F_1 [F_0 HF]and F_1 [F_0 HF-
964 LF] mice as determined by small RNA-seq. (**c,d**) Abundance of (**c**) *miR-143-3p*, *miR-181a-2-3p*, *miR-*
965 *378*, *miR-532-5p* and (**d**) *miR-let-7* isoforms in eWAT of F_1 [F_0 LF], F_1 [F_0 HF] and F_1 [F_0 HF-LF] mice.
966 An unpaired, two-tailed Student's t-test was used for statistical analysis in (**d**) and P values indicted.
967
968 **Figure S8: Obesity-associated miR-let-7 impairs adipocyte mitochondrial function via silencing**
969 **of DICER1.**
970 (**a**) Multidimensional scaling (MDS) plots of transcriptomic changes in 1°eWA transfected with
971 Negative Control (n=4), *miR-let-7d-5p* (n=4) and *miR-let-7e-5p* (n=4) mimetics as determined by
972 mRNA-seq. (**b**) GSEA-GOBP analysis of DEGs in 1°eWA transfected with Negative Control (n=4),
973 *miR-let-7d-5p* (n=4) and *miR-let-7e-5p* (n=4) mimics. (**c,d)** Western blot analysis (**c**) and densitometric
974 quantification (**d**) of indicated proteins in 1°eWA transfected with Negative Control, *miR-let-7d-5p* and
975 *miR-let-7e-5p* mimetics and analyzed using indicated antibodies. Heat shock protein (HSC) 70 antibody
976 was used as loading control and the blots shown are representative of three independent experiments.
977 Superscript letters represent group comparisions **a**, $p<0.05$ Negative Control vs *miR-let-7d-5p*; **b**,
978 $p<0.05$, *miR-let-7d-5p* vs *miR-let-7e-5p*; **c**, $p<0.05$, Negative Control vs *miR-let-7e-5p*). (**e**) *Dicer1*
979 mRNA levels in 1°eA after transfection with 100 nM Negative Control locked nucleic acids (LNA) and
980 two independent LNA inhibitors targeting *Dicer1* (Dicer1 LNA#1, Dicer1 LNA#2). Data represent
981 three independent experiments, with each experiment performed in three technical replicates. Unpaired,
982 two-tailed Student's T-tests were performed, and P values are indicated within the panel. (**f,g)** Western

983 blot analysis (**f**) and densitometric quantification (**g**) of DICER1 protein levels in 1°eWA transfected
984 after transfection with 100 nM Negative Control LNAs and two LNAs targeting *Dicer1*. Data represent
985 three independent experiments, with each experiment performed in three technical replicates. Unpaired,
986 two-tailed Student's T-tests were performed, and P values are indicated within the panel.

987 **References:**

988 1 Trerotola, M., Relli, V., Simeone, P. & Alberti, S. Epigenetic inheritance and the missing
989 heritability. *Human genomics* **9**, 17 (2015). https://doi.org:10.1186/s40246-015-0041-3
990 2 Bygren, L. O., Kaati, G. & Edvinsson, S. Longevity determined by paternal ancestors'
991 nutrition during their slow growth period. *Acta Biotheor* **49**, 53-59 (2001).
992 https://doi.org:10.1023/a:1010241825519
993 3 Pembrey, M. E. *et al.* Sex-specific, male-line transgenerational responses in humans.
994 *European journal of human genetics : EJHG* **14**, 159-166 (2006).
995 https://doi.org:10.1038/sj.ejhg.5201538
996 4 Lumey, L. H., Stein, A. D., Kahn, H. S. & Romijn, J. A. Lipid profiles in middle-aged men
997 and women after famine exposure during gestation: the Dutch Hunger Winter Families Study.
998 *Am J Clin Nutr* **89**, 1737-1743 (2009). https://doi.org:10.3945/ajcn.2008.27038
999 5 Carone, B. R. *et al.* Paternally induced transgenerational environmental reprogramming of
1000 metabolic gene expression in mammals. *Cell* **143**, 1084-1096 (2010).
1001 https://doi.org:10.1016/j.cell.2010.12.008
1002 6 Ng, S. F. *et al.* Paternal high-fat diet consumption induces common changes in the
1003 transcriptomes of retroperitoneal adipose and pancreatic islet tissues in female rat offspring.
1004 *FASEB journal : official publication of the Federation of American Societies for*
1005 *Experimental Biology* **28**, 1830-1841 (2014). https://doi.org:10.1096/fj.13-244046
1006 7 de Castro Barbosa, T. *et al.* High-fat diet reprograms the epigenome of rat spermatozoa and
1007 transgenerationally affects metabolism of the offspring. *Molecular metabolism* **5**, 184-197
1008 (2016). https://doi.org:10.1016/j.molmet.2015.12.002
1009 8 de Castro Barbosa, T., Alm, P. S., Krook, A., Barres, R. & Zierath, J. R. Paternal high-fat diet
1010 transgenerationally impacts hepatic immunometabolism. *FASEB journal : official publication*
1011 *of the Federation of American Societies for Experimental Biology* **33**, 6269-6280 (2019).
1012 https://doi.org:10.1096/fj.201801879RR
1013 9 Wang, Y. *et al.* Sperm microRNAs confer depression susceptibility to offspring. *Sci Adv* **7**
1014 (2021). https://doi.org:10.1126/sciadv.abd7605
1015 10 Dias, B. G. & Ressler, K. J. Parental olfactory experience influences behavior and neural
1016 structure in subsequent generations. *Nature neuroscience* **17**, 89-96 (2014).
1017 https://doi.org:10.1038/nn.3594
1018 11 Gapp, K. *et al.* Implication of sperm RNAs in transgenerational inheritance of the effects of
1019 early trauma in mice. *Nature neuroscience* **17**, 667-669 (2014).
1020 https://doi.org:10.1038/nn.3695
1021 12 Sun, W. *et al.* Cold-induced epigenetic programming of the sperm enhances brown adipose
1022 tissue activity in the offspring. *Nature medicine* **24**, 1372-1383 (2018).
1023 https://doi.org:10.1038/s41591-018-0102-y

1024 13 Skvortsova, K., Iovino, N. & Bogdanovic, O. Functions and mechanisms of epigenetic
1025 inheritance in animals. *Nature reviews. Molecular cell biology* **19**, 774-790 (2018).
1026 https://doi.org:10.1038/s41580-018-0074-2
1027 14 Rechavi, O., Minevich, G. & Hobert, O. Transgenerational inheritance of an acquired small
1028 RNA-based antiviral response in C. elegans. *Cell* **147**, 1248-1256 (2011).
1029 https://doi.org:10.1016/j.cell.2011.10.042
1030 15 Fire, A. *et al.* Potent and specific genetic interference by double-stranded RNA in
1031 Caenorhabditis elegans. *Nature* **391**, 806-811 (1998). https://doi.org:10.1038/35888
1032 16 Ashe, A. *et al.* piRNAs can trigger a multigenerational epigenetic memory in the germline of
1033 C. elegans. *Cell* **150**, 88-99 (2012). https://doi.org:10.1016/j.cell.2012.06.018
1034 17 de Vanssay, A. *et al.* Paramutation in Drosophila linked to emergence of a piRNA-producing
1035 locus. *Nature* **490**, 112-115 (2012). https://doi.org:10.1038/nature11416
1036 18 Rassoulzadegan, M. *et al.* RNA-mediated non-mendelian inheritance of an epigenetic change
1037 in the mouse. *Nature* **441**, 469-474 (2006). https://doi.org:10.1038/nature04674
1038 19 Gross, N., Kropp, J. & Khatib, H. MicroRNA Signaling in Embryo Development. *Biology*
1039 *(Basel)* **6** (2017). https://doi.org:10.3390/biology6030034
1040 20 Natt, D. *et al.* Human sperm displays rapid responses to diet. *PLoS Biol* **17**, e3000559 (2019).
1041 https://doi.org:10.1371/journal.pbio.3000559
1042 21 Tomar, A. *et al.* Epigenetic inheritance of diet-induced and sperm-borne mitochondrial
1043 RNAs. *Nature* **630**, 720-727 (2024). https://doi.org:10.1038/s41586-024-07472-3
1044 22 Grandjean, V. *et al.* RNA-mediated paternal heredity of diet-induced obesity and metabolic
1045 disorders. *Scientific reports* **5**, 18193 (2015). https://doi.org:10.1038/srep18193
1046 23 Rodgers, A. B., Morgan, C. P., Leu, N. A. & Bale, T. L. Transgenerational epigenetic
1047 programming via sperm microRNA recapitulates effects of paternal stress. *Proceedings of the*
1048 *National Academy of Sciences of the United States of America* **112**, 13699-13704 (2015).
1049 https://doi.org:10.1073/pnas.1508347112
1050 24 Sharma, U. *et al.* Biogenesis and function of tRNA fragments during sperm maturation and
1051 fertilization in mammals. *Science* (2015). https://doi.org:10.1126/science.aad6780
1052 25 Korhonen, H. M. *et al.* Dicer is required for haploid male germ cell differentiation in mice.
1053 *PloS one* **6**, e24821 (2011). https://doi.org:10.1371/journal.pone.0024821
1054 26 Bernstein, E. *et al.* Dicer is essential for mouse development. *Nature genetics* **35**, 215-217
1055 (2003). https://doi.org:10.1038/ng1253
1056 27 Chen, Q. *et al.* Sperm tsRNAs contribute to intergenerational inheritance of an acquired
1057 metabolic disorder. *Science* (2015). https://doi.org:10.1126/science.aad7977
1058 28 Rodgers, A. B., Morgan, C. P., Bronson, S. L., Revello, S. & Bale, T. L. Paternal stress
1059 exposure alters sperm microRNA content and reprograms offspring HPA stress axis

1060 regulation. *The Journal of neuroscience : the official journal of the Society for Neuroscience*
1061 **33**, 9003-9012 (2013). https://doi.org:10.1523/JNEUROSCI.0914-13.2013
1062 29 Cropley, J. E., Suter, C. M., Beckman, K. B. & Martin, D. I. Germ-line epigenetic
1063 modification of the murine A vy allele by nutritional supplementation. *Proceedings of the*
1064 *National Academy of Sciences of the United States of America* **103**, 17308-17312 (2006).
1065 https://doi.org:10.1073/pnas.0607090103
1066 30 Zhang, Y., Shi, J., Rassoulzadegan, M., Tuorto, F. & Chen, Q. Sperm RNA code programmes
1067 the metabolic health of offspring. *Nature reviews. Endocrinology* **15**, 489-498 (2019).
1068 https://doi.org:10.1038/s41574-019-0226-2
1069 31 Sun, K., Kusminski, C. M. & Scherer, P. E. Adipose tissue remodeling and obesity. *The*
1070 *Journal of clinical investigation* **121**, 2094-2101 (2011). https://doi.org:10.1172/JCI45887
1071 32 Scherer, P. E. Adipose tissue: from lipid storage compartment to endocrine organ. *Diabetes*
1072 **55**, 1537-1545 (2006). https://doi.org:10.2337/db06-0263
1073 33 Lee, J. H. *et al.* The Role of Adipose Tissue Mitochondria: Regulation of Mitochondrial
1074 Function for the Treatment of Metabolic Diseases. *Int J Mol Sci* **20** (2019).
1075 https://doi.org:10.3390/ijms20194924
1076 34 Czech, M. P. Mechanisms of insulin resistance related to white, beige, and brown adipocytes.
1077 *Molecular metabolism* **34**, 27-42 (2020). https://doi.org:10.1016/j.molmet.2019.12.014
1078 35 Kahn, C. R., Wang, G. & Lee, K. Y. Altered adipose tissue and adipocyte function in the
1079 pathogenesis of metabolic syndrome. *The Journal of clinical investigation* **129**, 3990-4000
1080 (2019). https://doi.org:10.1172/JCI129187
1081 36 Bartelt, A. & Heeren, J. Adipose tissue browning and metabolic health. *Nature reviews.*
1082 *Endocrinology* **10**, 24-36 (2014). https://doi.org:10.1038/nrendo.2013.204
1083 37 Schottl, T., Kappler, L., Braun, K., Fromme, T. & Klingenspor, M. Limited mitochondrial
1084 capacity of visceral versus subcutaneous white adipocytes in male C57BL/6N mice.
1085 *Endocrinology* **156**, 923-933 (2015). https://doi.org:10.1210/en.2014-1689
1086 38 Heinonen, S., Jokinen, R., Rissanen, A. & Pietilainen, K. H. White adipose tissue
1087 mitochondrial metabolism in health and in obesity. *Obes Rev* **21**, e12958 (2020).
1088 https://doi.org:10.1111/obr.12958
1089 39 Kusminski, C. M. *et al.* MitoNEET-driven alterations in adipocyte mitochondrial activity
1090 reveal a crucial adaptive process that preserves insulin sensitivity in obesity. *Nature medicine*
1091 **18**, 1539-1549 (2012). https://doi.org:10.1038/nm.2899
1092 40 Gonzalez-Franquesa, A. *et al.* Remission of obesity and insulin resistance is not sufficient to
1093 restore mitochondrial homeostasis in visceral adipose tissue. *Redox Biol* **54**, 102353 (2022).
1094 https://doi.org:10.1016/j.redox.2022.102353
1095 41 Schottl, T., Kappler, L., Fromme, T. & Klingenspor, M. Limited OXPHOS capacity in white
1096 adipocytes is a hallmark of obesity in laboratory mice irrespective of the glucose tolerance

1097 status. *Molecular metabolism* **4**, 631-642 (2015).
1098 https://doi.org:10.1016/j.molmet.2015.07.001
1099 42 Soro-Arnaiz, I. *et al.* Role of Mitochondrial Complex IV in Age-Dependent Obesity. *Cell*
1100 *reports* **16**, 2991-3002 (2016). https://doi.org:10.1016/j.celrep.2016.08.041
1101 43 Wang, Y. *et al.* Metformin Improves Mitochondrial Respiratory Activity through Activation
1102 of AMPK. *Cell reports* **29**, 1511-1523 e1515 (2019).
1103 https://doi.org:10.1016/j.celrep.2019.09.070
1104 44 Borralho, P. M., Rodrigues, C. M. & Steer, C. J. microRNAs in Mitochondria: An
1105 Unexplored Niche. *Adv Exp Med Biol* **887**, 31-51 (2015). https://doi.org:10.1007/978-3-319-
1106 22380-3_3
1107 45 Bandiera, S. *et al.* Nuclear outsourcing of RNA interference components to human
1108 mitochondria. *PloS one* **6**, e20746 (2011). https://doi.org:10.1371/journal.pone.0020746
1109 46 Barrey, E. *et al.* Pre-microRNA and mature microRNA in human mitochondria. *PloS one* **6**,
1110 e20220 (2011). https://doi.org:10.1371/journal.pone.0020220
1111 47 Mori, M. A. *et al.* Role of MicroRNA Processing in Adipose Tissue in Stress Defense and
1112 Longevity. *Cell metabolism* **16**, 336-347 (2012). https://doi.org:S1550-4131(12)00322-1 [pii]
1113 10.1016/j.cmet.2012.07.017
1114 48 Mori, M. A. *et al.* Altered miRNA processing disrupts brown/white adipocyte determination
1115 and associates with lipodystrophy. *The Journal of clinical investigation* **124**, 3339-3351
1116 (2014). https://doi.org:10.1172/JCI73468
1117 49 Oliverio, M. *et al.* Dicer1-miR-328-Bace1 signalling controls brown adipose tissue
1118 differentiation and function. *Nature cell biology* **18**, 328-336 (2016).
1119 https://doi.org:10.1038/ncb3316
1120 50 Turner, N. *et al.* A selective inhibitor of ceramide synthase 1 reveals a novel role in fat
1121 metabolism. *Nature communications* **9**, 3165 (2018). https://doi.org:10.1038/s41467-018-
1122 05613-7
1123 51 Subramanian, A. *et al.* Gene set enrichment analysis: a knowledge-based approach for
1124 interpreting genome-wide expression profiles. *Proceedings of the National Academy of*
1125 *Sciences of the United States of America* **102**, 15545-15550 (2005).
1126 https://doi.org:0506580102 [pii]
1127 10.1073/pnas.0506580102
1128 52 Brieno-Enriquez, M. A. *et al.* Exposure to endocrine disruptor induces transgenerational
1129 epigenetic deregulation of microRNAs in primordial germ cells. *PloS one* **10**, e0124296
1130 (2015). https://doi.org:10.1371/journal.pone.0124296
1131 53 Zhu, H. *et al.* The Lin28/let-7 axis regulates glucose metabolism. *Cell* **147**, 81-94 (2011).
1132 https://doi.org:10.1016/j.cell.2011.08.033

1133 54 Frost, R. J. & Olson, E. N. Control of glucose homeostasis and insulin sensitivity by the Let-7
1134 family of microRNAs. *Proceedings of the National Academy of Sciences of the United States*
1135 *of America* **108**, 21075-21080 (2011). https://doi.org:10.1073/pnas.1118922109
1136 55 Giroud, M. *et al.* Let-7i-5p represses brite adipocyte function in mice and humans. *Scientific*
1137 *reports* **6**, 28613 (2016). https://doi.org:10.1038/srep28613
1138 56 O'Connor, S. *et al.* AGO HITS-CLIP reveals distinct miRNA regulation of white and brown
1139 adipose tissue identity. *Genes & development* (2021). https://doi.org:10.1101/gad.345447.120
1140 57 Fullston, T. *et al.* Paternal obesity initiates metabolic disturbances in two generations of mice
1141 with incomplete penetrance to the F2 generation and alters the transcriptional profile of testis
1142 and sperm microRNA content. *FASEB journal : official publication of the Federation of*
1143 *American Societies for Experimental Biology* **27**, 4226-4243 (2013).
1144 https://doi.org:10.1096/fj.12-224048
1145 58 Liu, W. *et al.* Expression of microRNA let-7 in cleavage embryos modulates cell fate
1146 determination and formation of mouse blastocystsdagger. *Biol Reprod* **107**, 1452-1463
1147 (2022). https://doi.org:10.1093/biolre/ioac181
1148 59 Cheong, A. W. *et al.* MicroRNA Let-7a and dicer are important in the activation and
1149 implantation of delayed implanting mouse embryos. *Human reproduction* **29**, 750-762
1150 (2014). https://doi.org:10.1093/humrep/det462
1151 60 Tobi, E. W. *et al.* DNA methylation signatures link prenatal famine exposure to growth and
1152 metabolism. *Nature communications* **5**, 5592 (2014). https://doi.org:10.1038/ncomms6592
1153 61 Schulz, L. C. The Dutch Hunger Winter and the developmental origins of health and disease.
1154 *Proceedings of the National Academy of Sciences of the United States of America* **107**, 16757-
1155 16758 (2010). https://doi.org:10.1073/pnas.1012911107
1156 62 Jepsen, I. E. *et al.* Turning waiting time into treatment time: Weight reduction by a lifestyle
1157 intervention programme for patients with obesity before fertility treatment. *Reproductive,*
1158 *Female and Child Health* **2**, 133-142 (2023). https://doi.org:https://doi.org/10.1002/rfc2.46
1159 63 Yuan, S. *et al.* Sperm-borne miRNAs and endo-siRNAs are important for fertilization and
1160 preimplantation embryonic development. *Development* **143**, 635-647 (2016).
1161 https://doi.org:10.1242/dev.131755
1162 64 Suh, N. & Blelloch, R. Small RNAs in early mammalian development: from gametes to
1163 gastrulation. *Development* **138**, 1653-1661 (2011). https://doi.org:10.1242/dev.056234
1164 65 Pfisterer, U. *et al.* Identification of epilepsy-associated neuronal subtypes and gene expression
1165 underlying epileptogenesis. *Nature communications* **11**, 5038 (2020).
1166 https://doi.org:10.1038/s41467-020-18752-7
1167 66 Popov, L. D. Mitochondrial biogenesis: An update. *J Cell Mol Med* **24**, 4892-4899 (2020).
1168 https://doi.org:10.1111/jcmm.15194

1169 67 Brandao, B. B. *et al.* Dynamic changes in DICER levels in adipose tissue control metabolic
1170 adaptations to exercise. *Proceedings of the National Academy of Sciences of the United States*
1171 *of America* **117**, 23932-23941 (2020). https://doi.org:10.1073/pnas.2011243117
1172 68 Sullivan, R. & Saez, F. Epididymosomes, prostasomes, and liposomes: their roles in
1173 mammalian male reproductive physiology. *Reproduction* **146**, R21-35 (2013).
1174 https://doi.org:10.1530/REP-13-0058
1175 69 Tan, K. *et al.* Downregulation of miR-199a-5p Disrupts the Developmental Potential of In
1176 Vitro-Fertilized Mouse Blastocysts. *Biol Reprod* **95**, 54 (2016).
1177 https://doi.org:10.1095/biolreprod.116.141051
1178 70 Chambers, M. C. *et al.* A cross-platform toolkit for mass spectrometry and proteomics.
1179 *Nature biotechnology* **30**, 918-920 (2012). https://doi.org:10.1038/nbt.2377
1180 71 Kind, T. *et al.* LipidBlast in silico tandem mass spectrometry database for lipid identification.
1181 *Nature methods* **10**, 755-758 (2013). https://doi.org:10.1038/nmeth.2551
1182 72 Luan, H., Ji, F., Chen, Y. & Cai, Z. statTarget: A streamlined tool for signal drift correction
1183 and interpretations of quantitative mass spectrometry-based omics data. *Anal Chim Acta*
1184 **1036**, 66-72 (2018). https://doi.org:10.1016/j.aca.2018.08.002
1185 73 Kleiner, D. E. *et al.* Design and validation of a histological scoring system for nonalcoholic
1186 fatty liver disease. *Hepatology* **41**, 1313-1321 (2005). https://doi.org:10.1002/hep.20701
1187 74 Rappsilber, J. & Mann, M. Analysis of the topology of protein complexes using cross-linking
1188 and mass spectrometry. *CSH Protoc* **2007**, pdb prot4594 (2007).
1189 https://doi.org:10.1101/pdb.prot4594
1190 75 Tyanova, S., Mann, M. & Cox, J. MaxQuant for in-depth analysis of large SILAC datasets.
1191 *Methods in molecular biology* **1188**, 351-364 (2014). https://doi.org:10.1007/978-1-4939-
1192 1142-4_24
1193 76 Tyanova, S. *et al.* The Perseus computational platform for comprehensive analysis of
1194 (prote)omics data. *Nature methods* **13**, 731-740 (2016). https://doi.org:10.1038/nmeth.3901
1195 77 Frankish, A. *et al.* GENCODE reference annotation for the human and mouse genomes.
1196 *Nucleic acids research* **47**, D766-D773 (2019). https://doi.org:10.1093/nar/gky955
1197 78 Dobin, A. *et al.* STAR: ultrafast universal RNA-seq aligner. *Bioinformatics* **29**, 15-21 (2013).
1198 https://doi.org:10.1093/bioinformatics/bts635
1199 79 Liao, Y., Smyth, G. K. & Shi, W. featureCounts: an efficient general purpose program for
1200 assigning sequence reads to genomic features. *Bioinformatics* **30**, 923-930 (2014).
1201 https://doi.org:10.1093/bioinformatics/btt656
1202 80 Robinson, M. D., McCarthy, D. J. & Smyth, G. K. edgeR: a Bioconductor package for
1203 differential expression analysis of digital gene expression data. *Bioinformatics* **26**, 139-140
1204 (2010). https://doi.org:10.1093/bioinformatics/btp616

1205 81 Law, C. W., Chen, Y., Shi, W. & Smyth, G. K. voom: Precision weights unlock linear model
1206 analysis tools for RNA-seq read counts. *Genome biology* **15**, R29 (2014).
1207 https://doi.org:10.1186/gb-2014-15-2-r29
1208 82 Wu, T. *et al.* clusterProfiler 4.0: A universal enrichment tool for interpreting omics data.
1209 *Innovation (Camb)* **2**, 100141 (2021). https://doi.org:10.1016/j.xinn.2021.100141
1210

Figure 1: Obesity and weight loss elicit reversible changes in glucose metabolism and mitochondrial metabolites

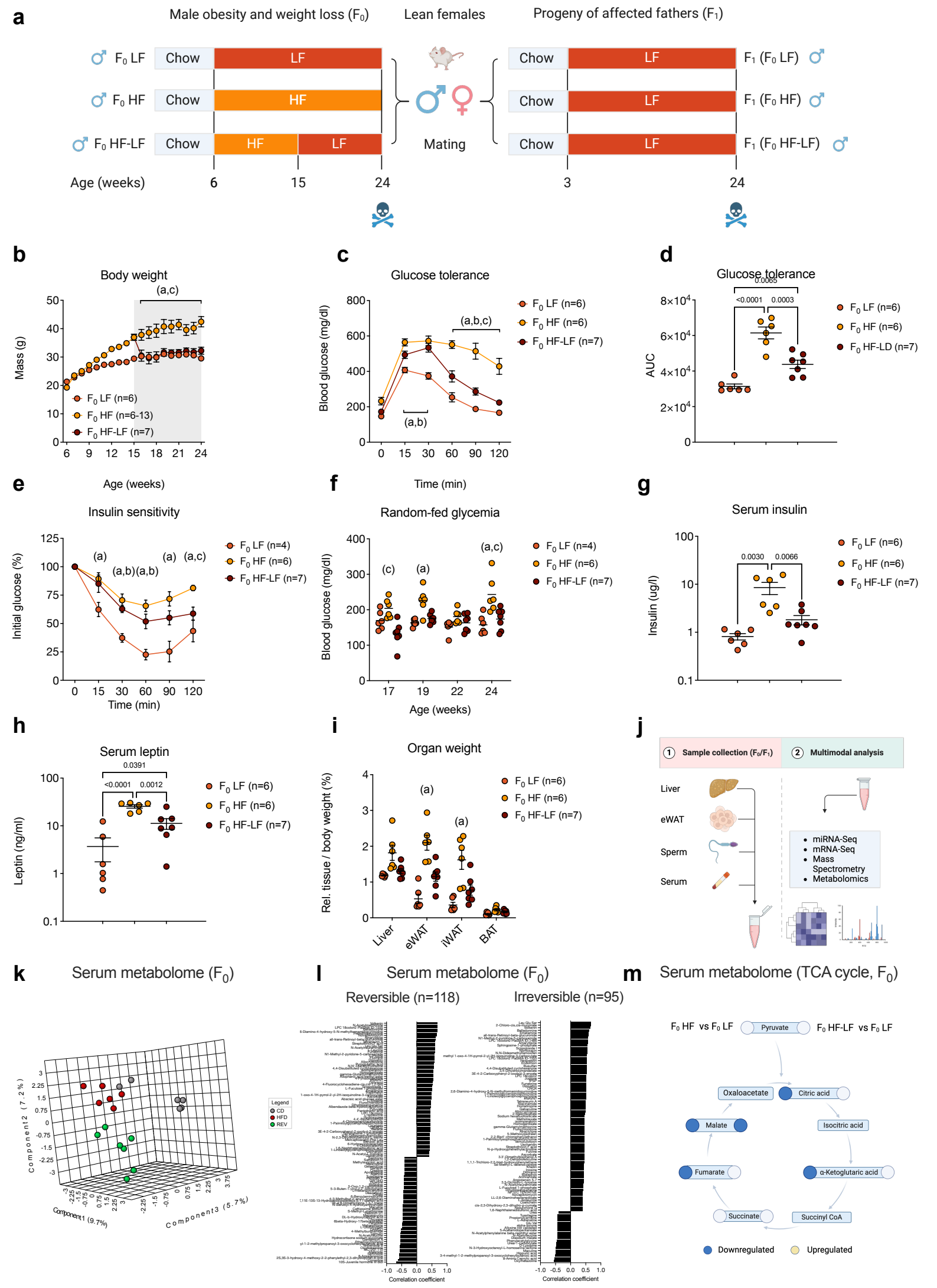

Figure 2: Multimodal omics analysis reveals reversible mitochondrial gene aberrations in obese adipose tisue

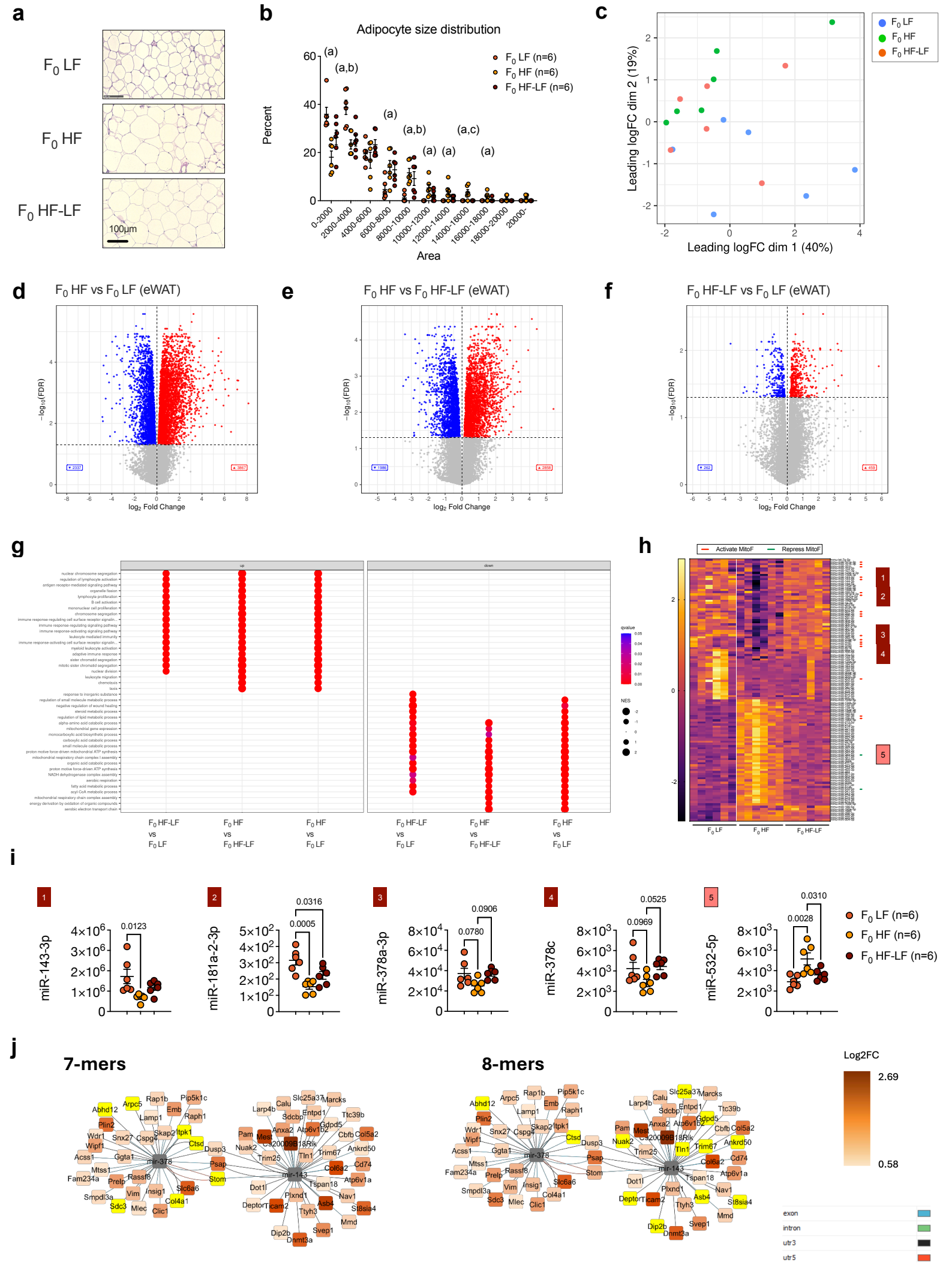

Figure 3: Paternal obesity impairs glucose tolerance and instigates adipose dysfunction in F_1 adipose tissue.

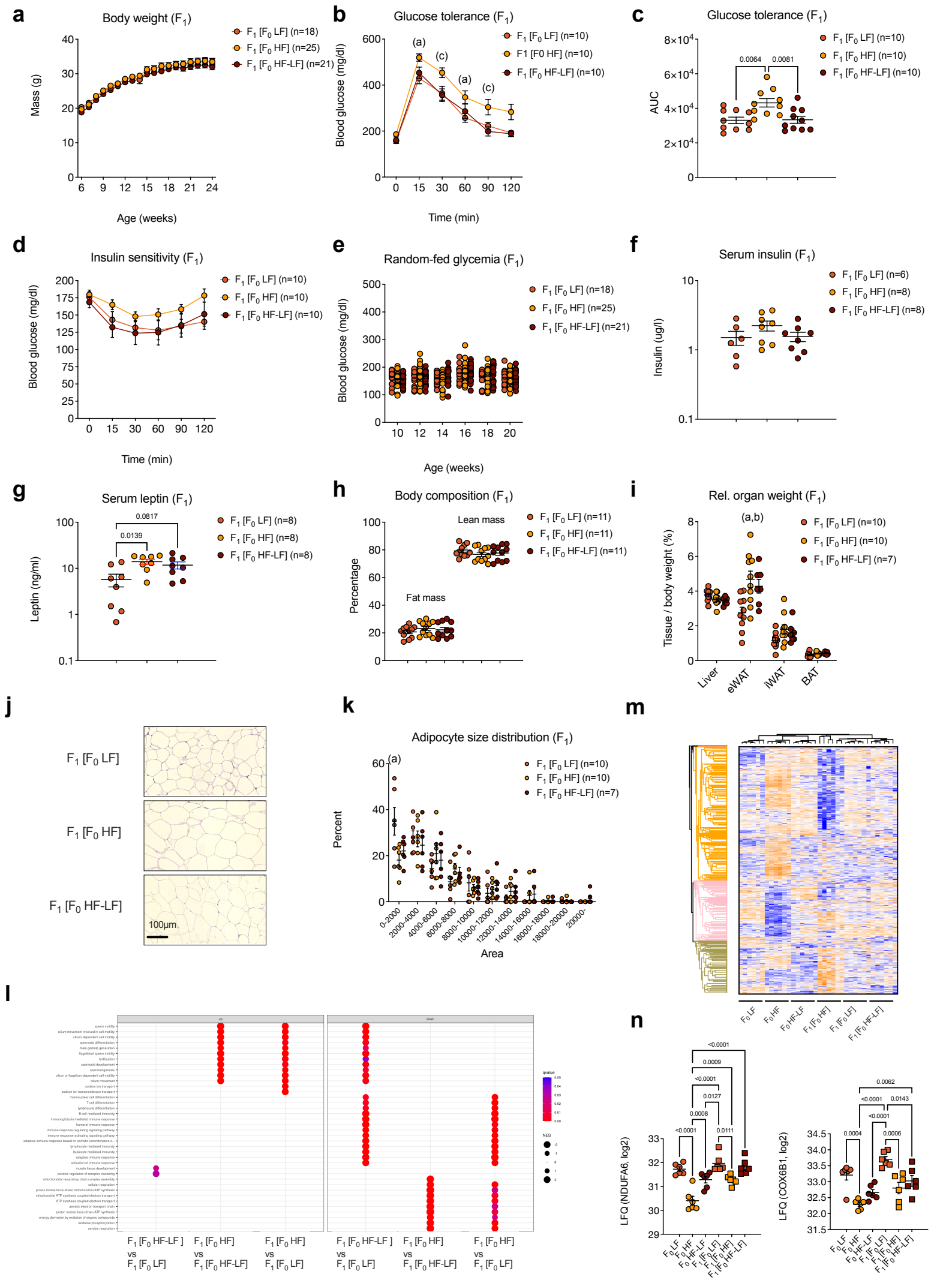

Figure 4: Obesity induces adipose tissue miR-let-7 and blunts mitochondrial function via a novel miR-let-7-DICER1 axis.

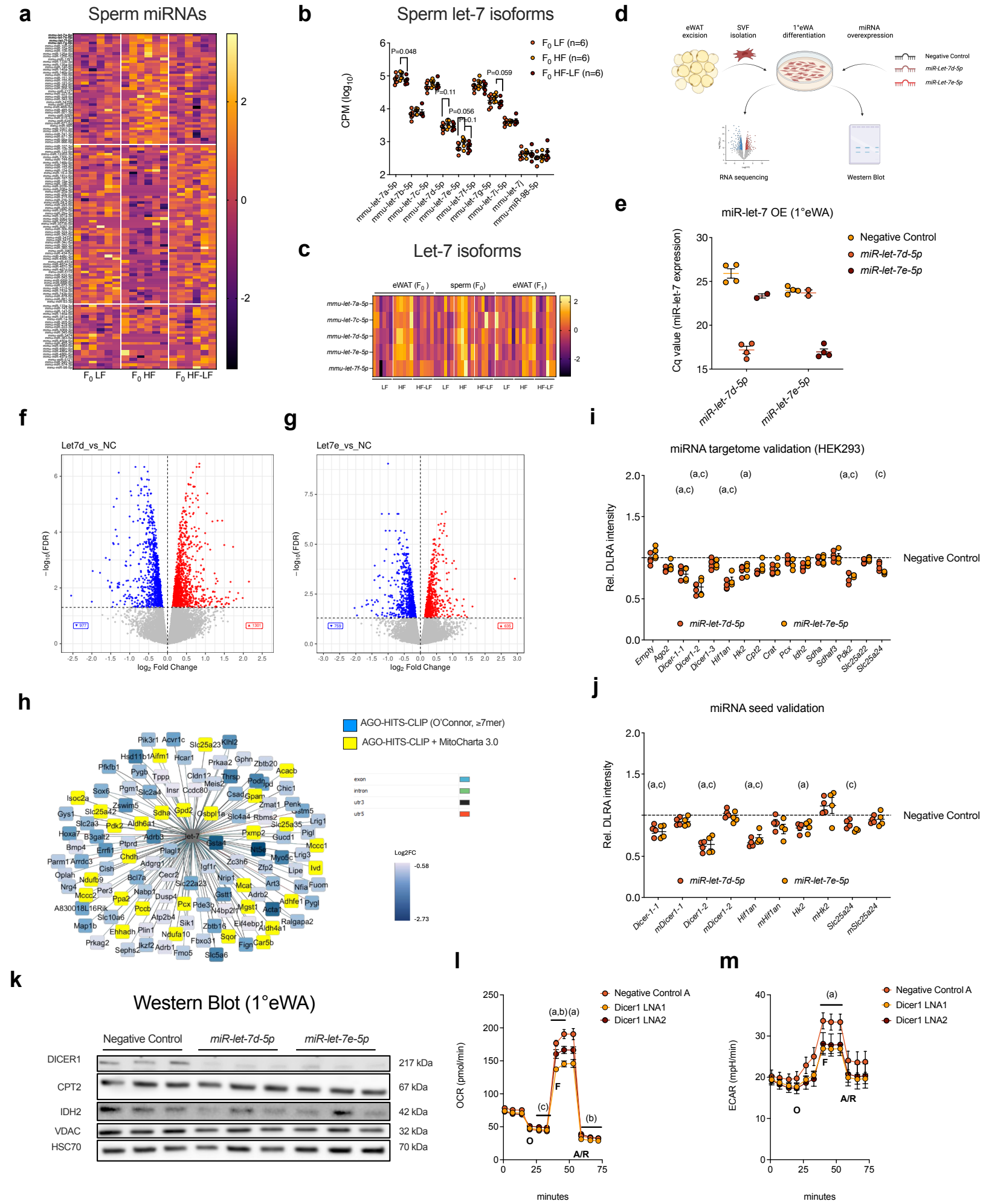

Figure 5: Zygotic microinjection of obesity-associated miR-let-7 causes glucose tolerance in sired mice.

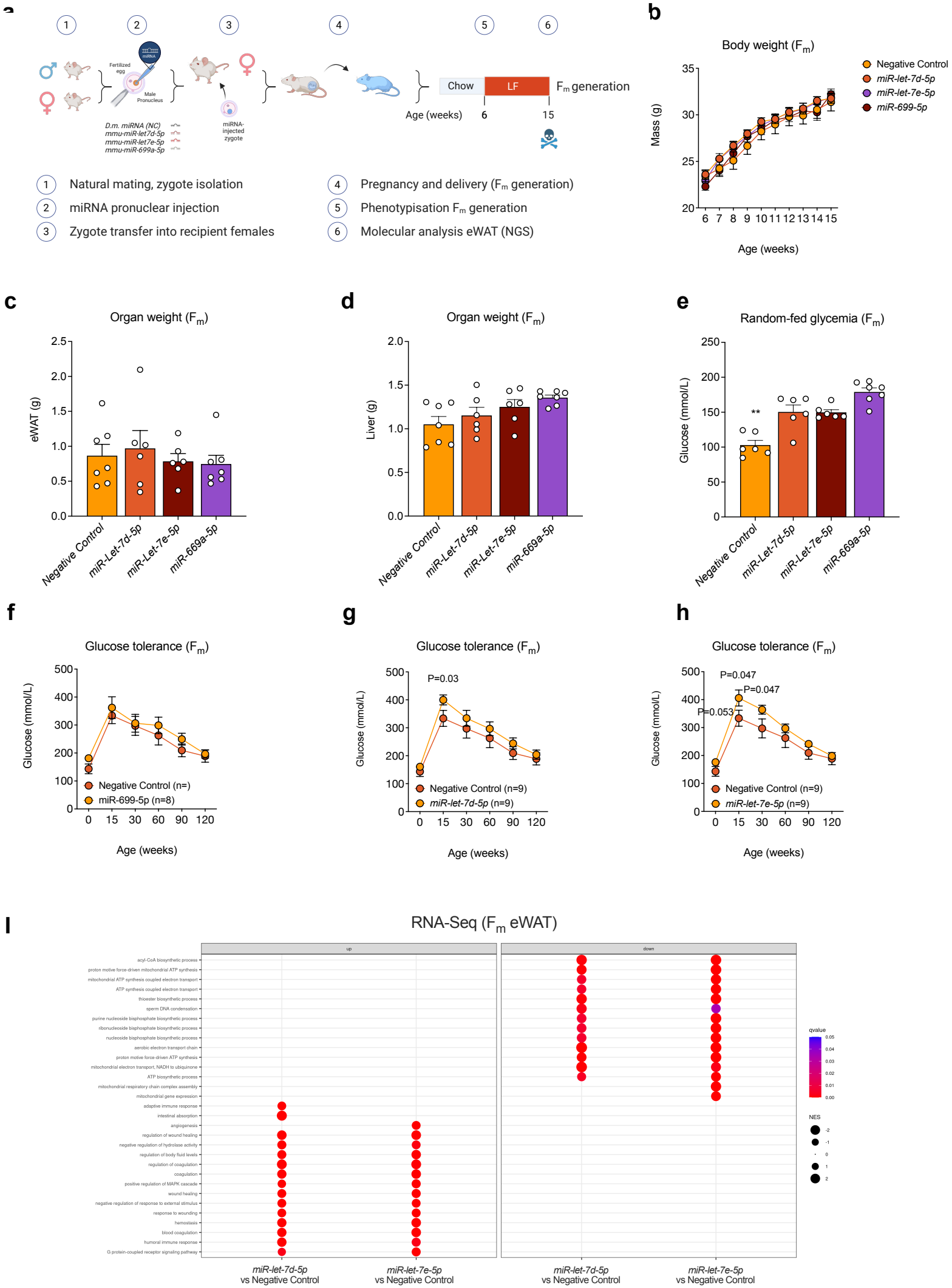

Figure 6: Obesity-associated miR-let-7 rewires mitochondrial metabolism during embryogenesis

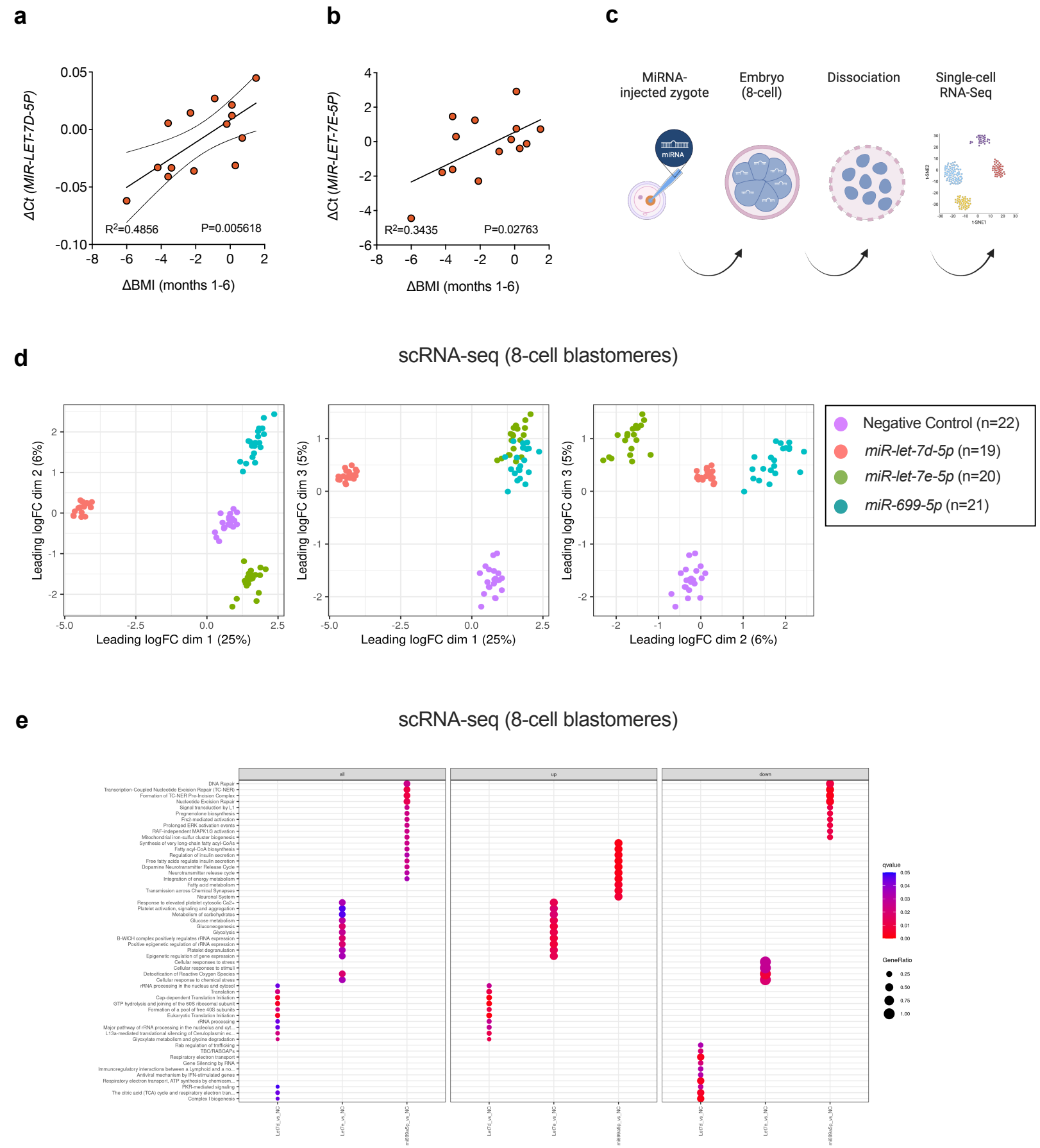

Figure S1: Obesity and weight loss elicits reversible changes in metabolites associated with mitochondrial function.

a TCA intermediate metabolites

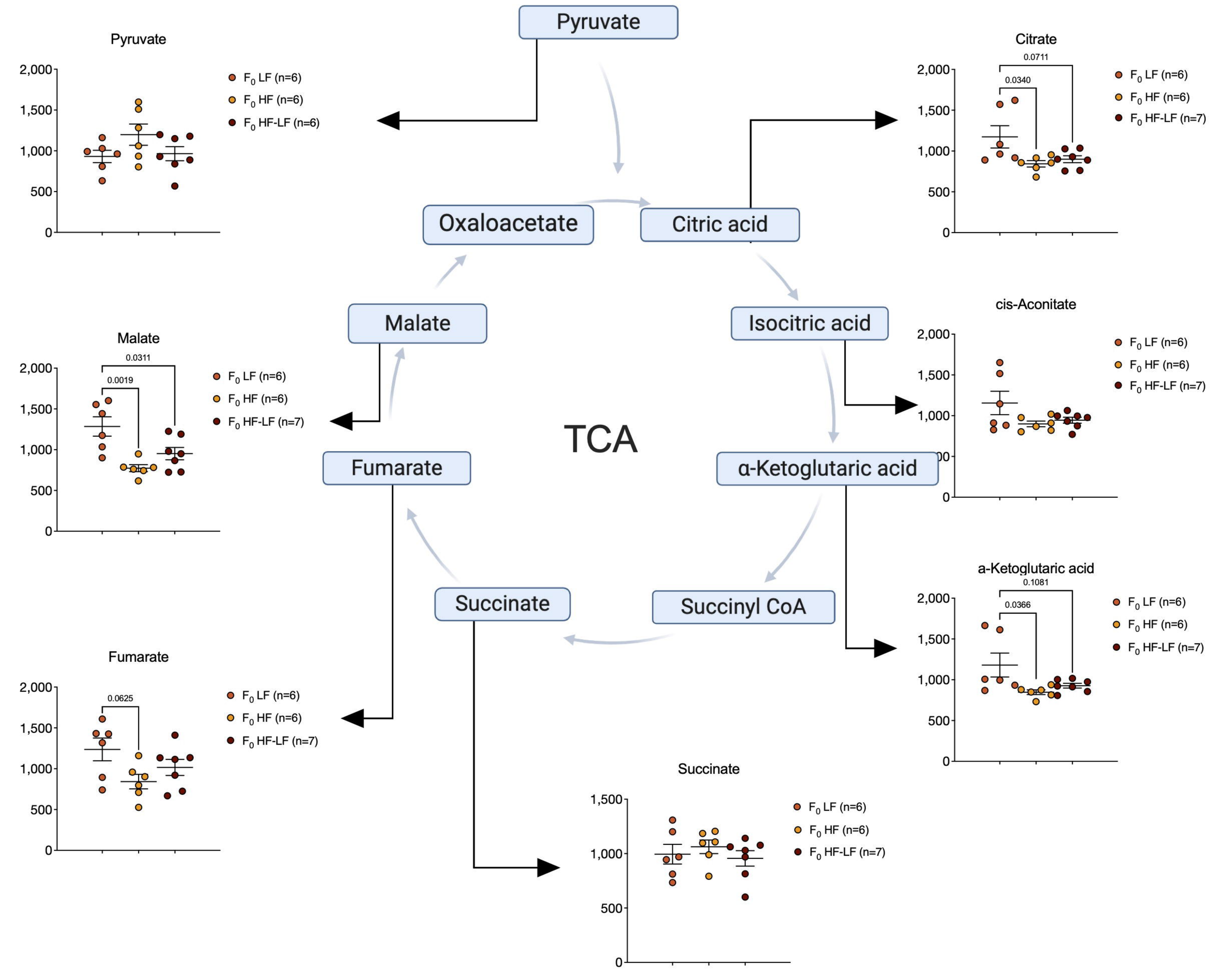

b Acylcarnitines

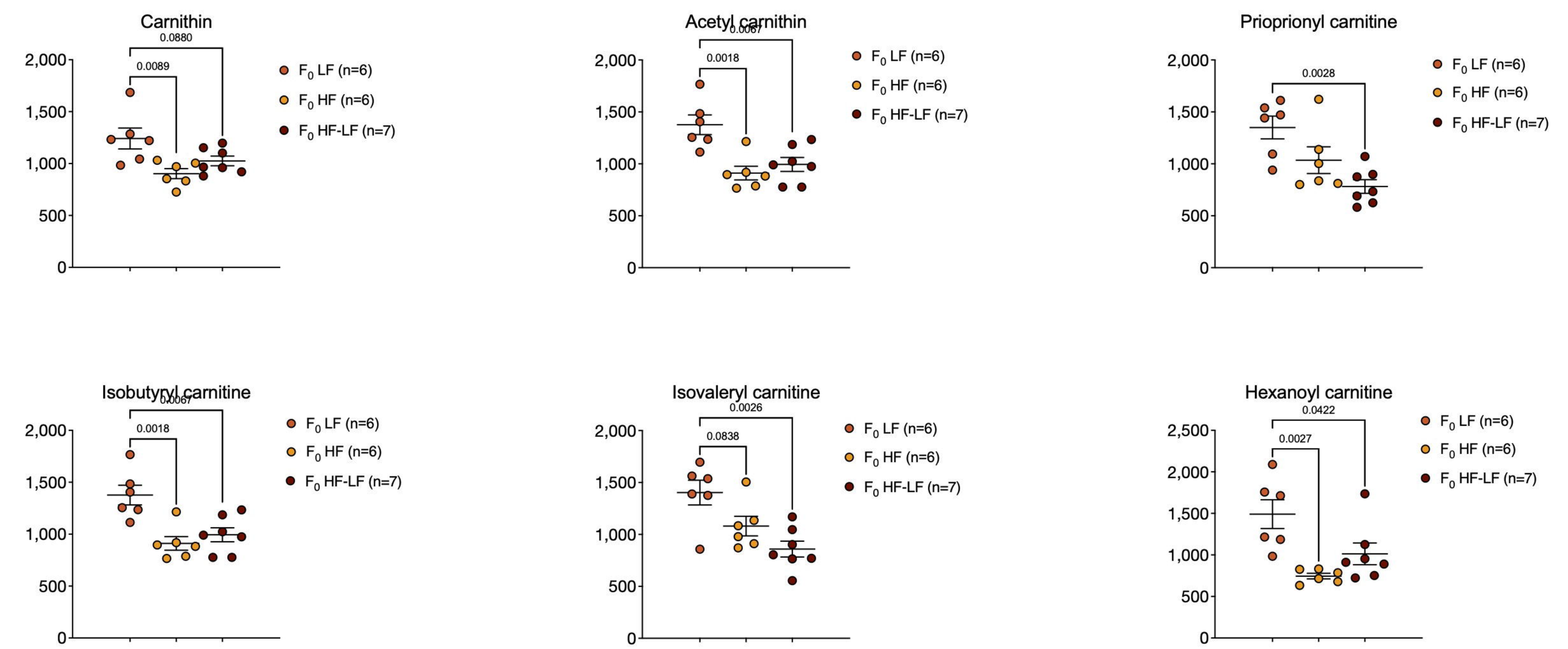

Figure S2: Obesity and weight loss elicits reversible changes in serum lipids controlling mitochondrial activity

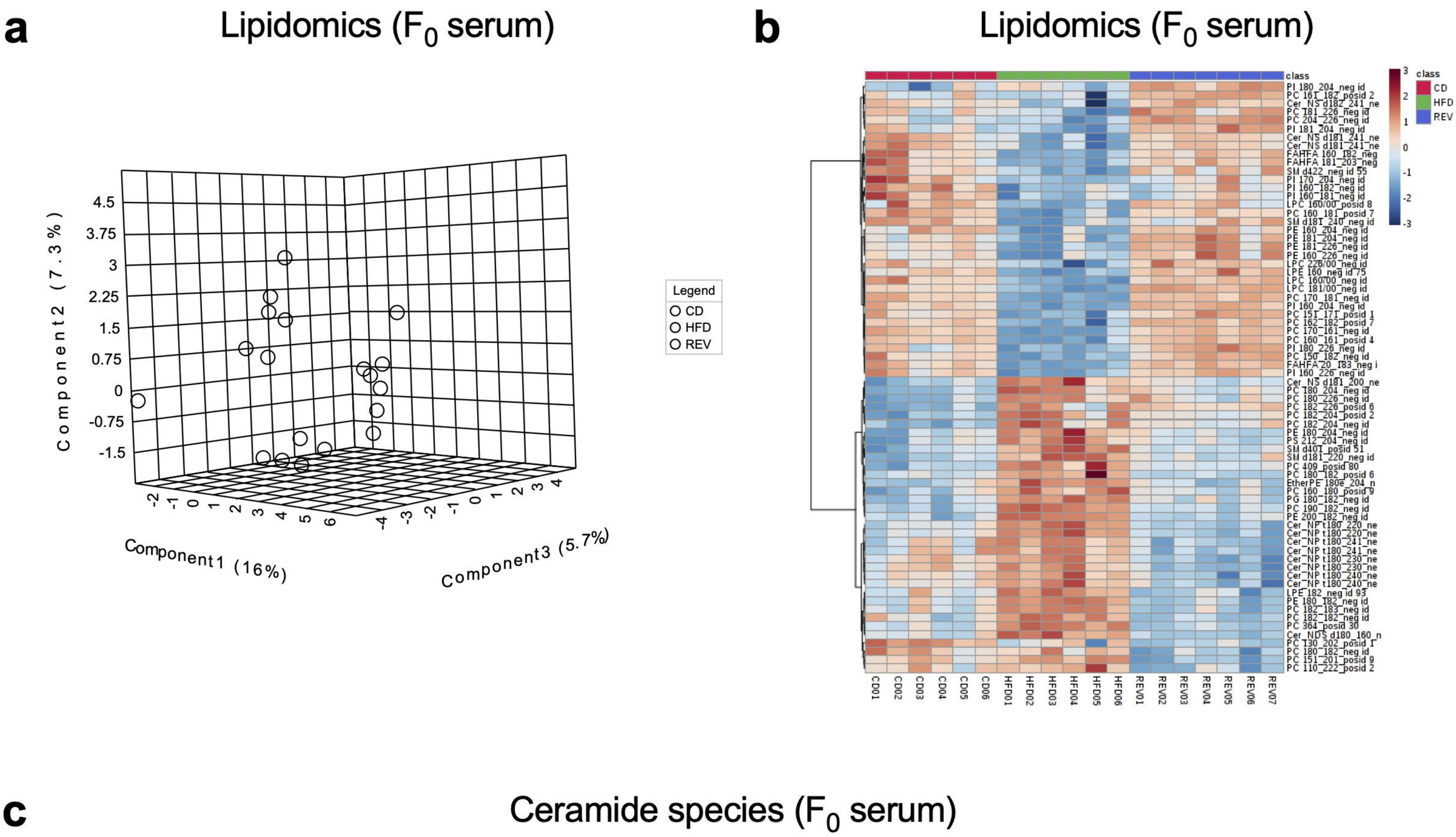

Figure S3: Paternal obesity and weight loss cause irreversible gene alterations in F_0 liver

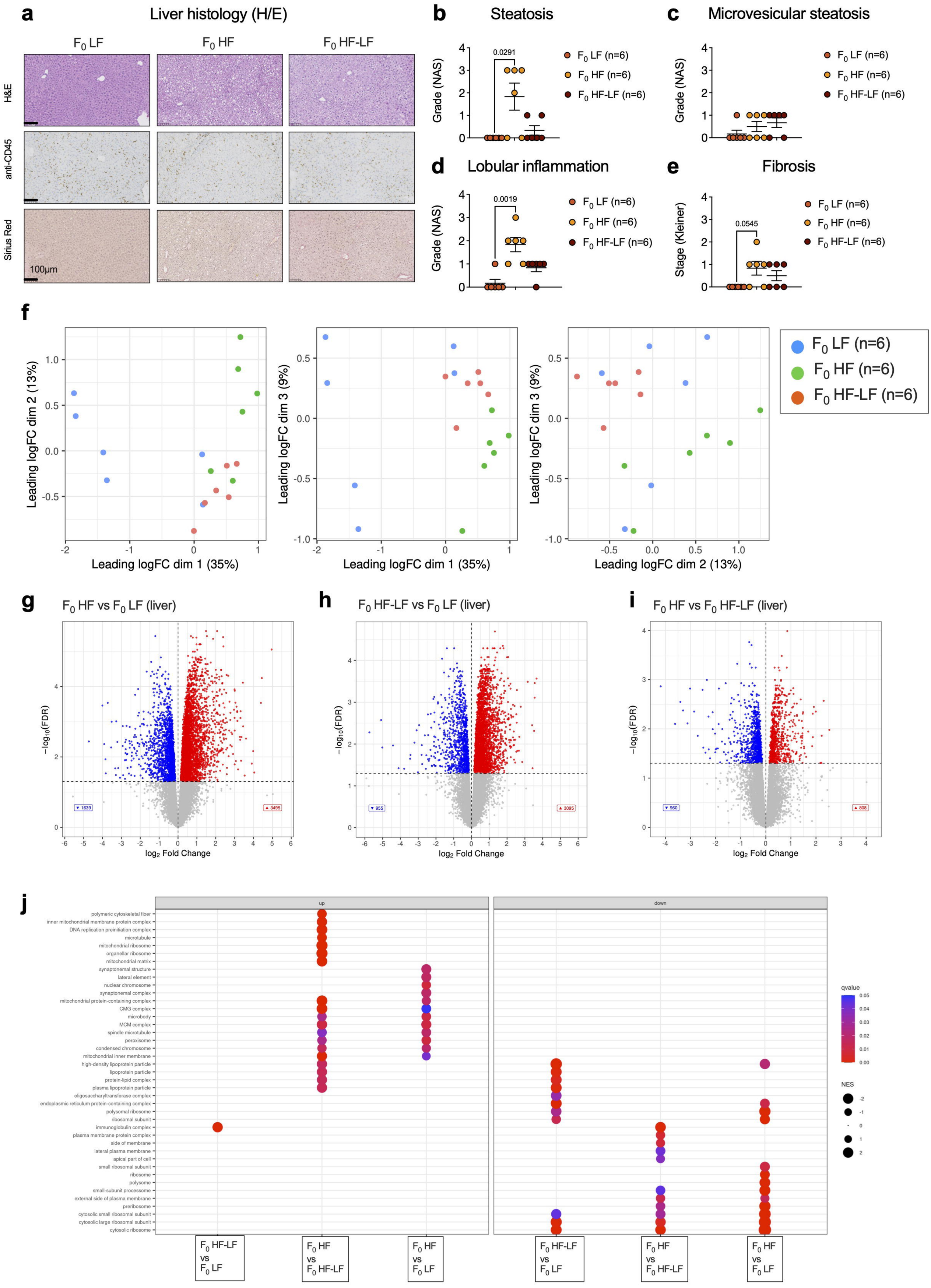

Figure S4: Reversible mitochondrial alterations in obese F_0 adipose tissue

a

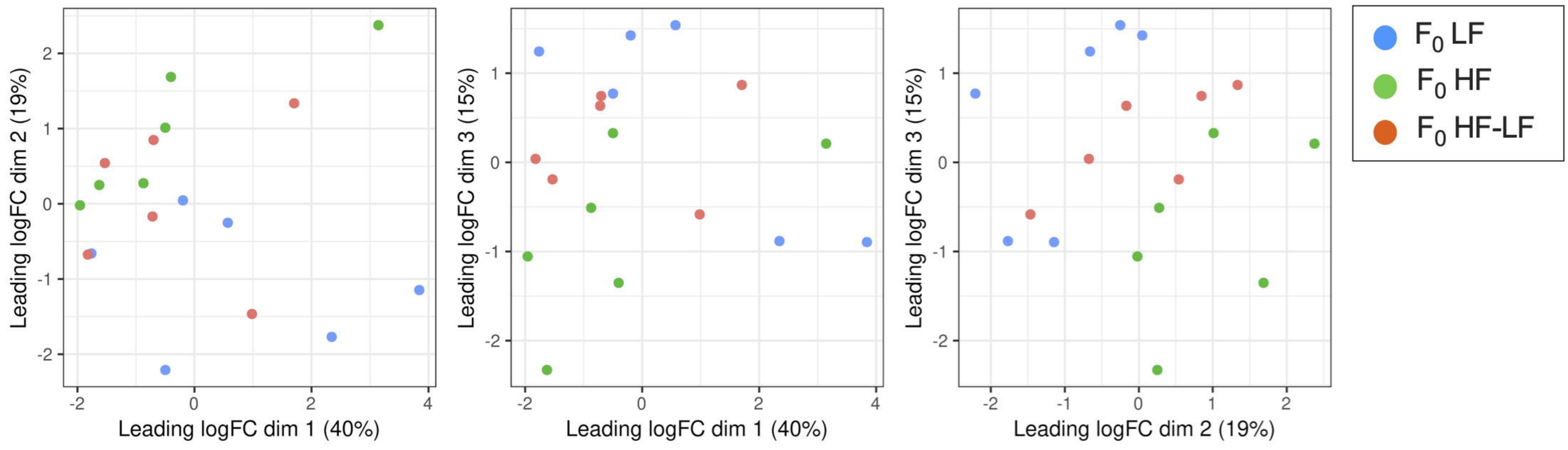

b

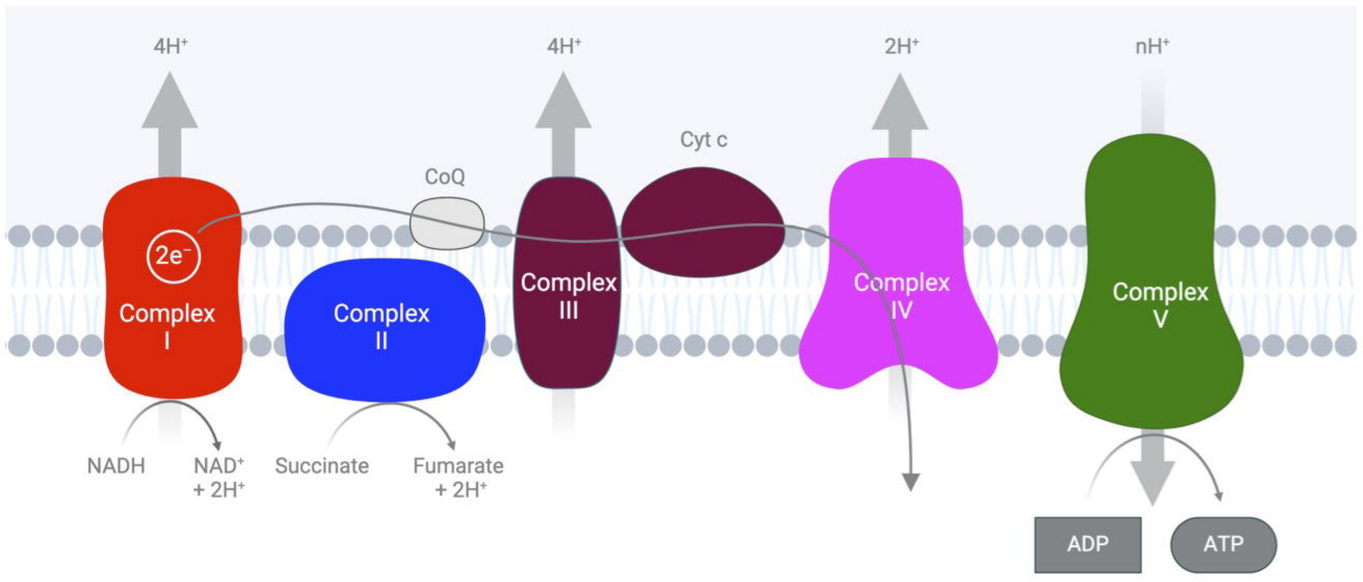

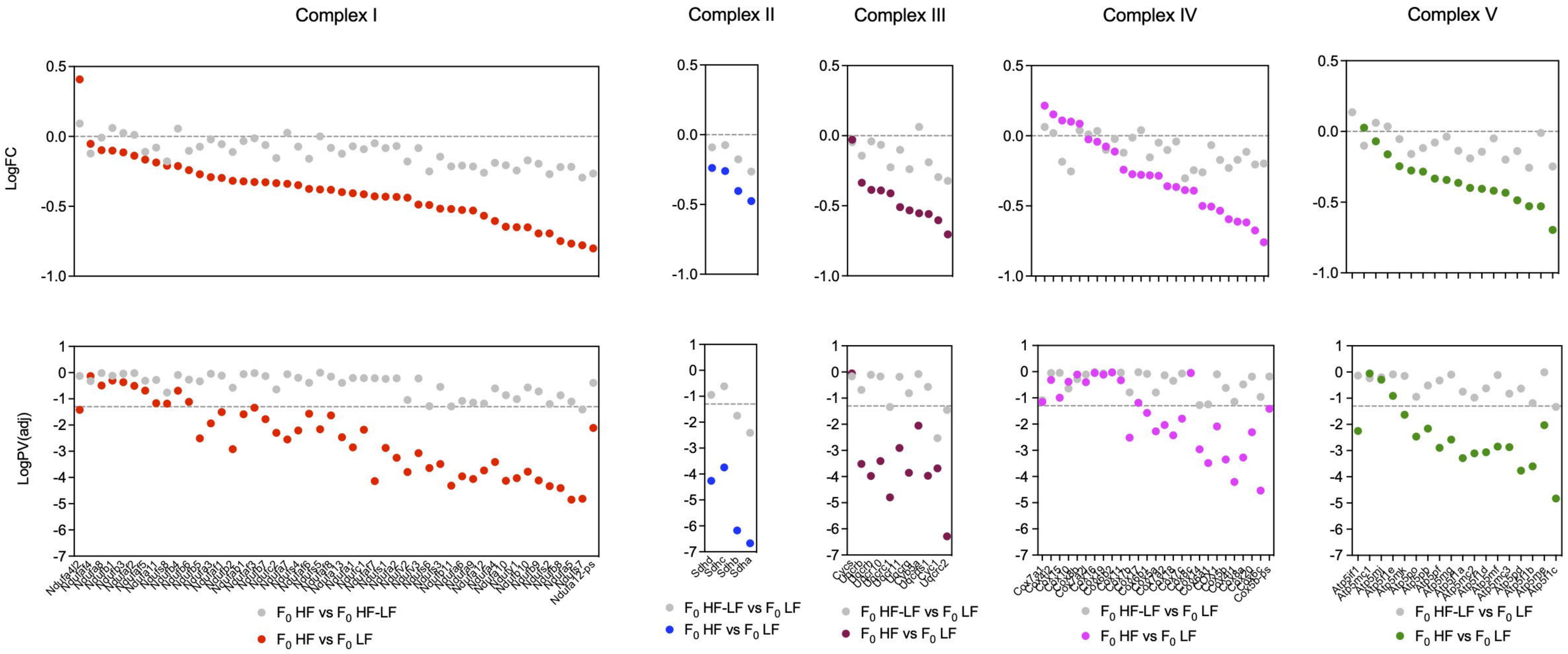

Figure S5: Reversible mitochondrial alterations in F_1 adipose tissue

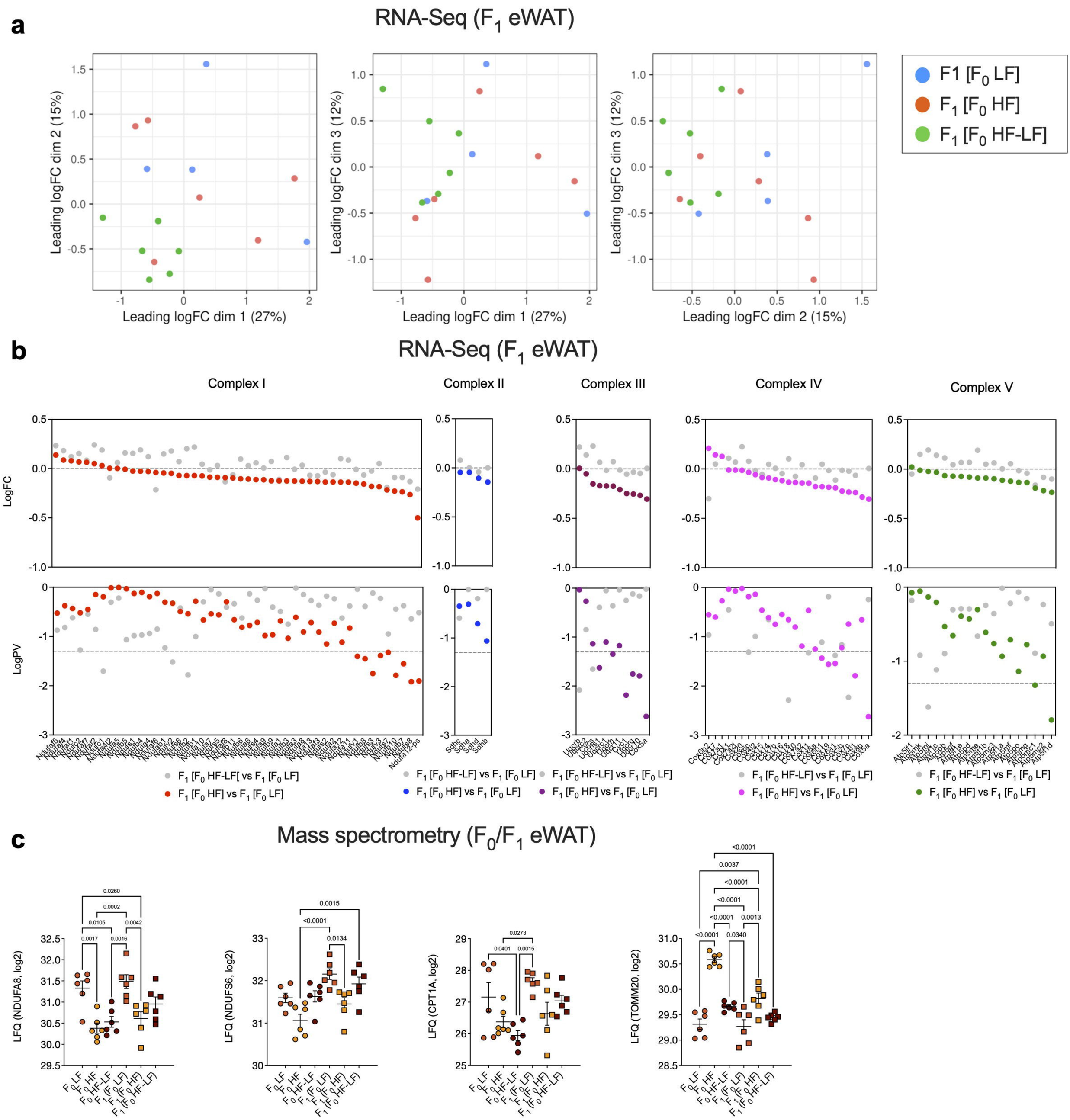

Figure S6: Paternal obesity and weight loss cause irreversible gene alterations in F_1 liver

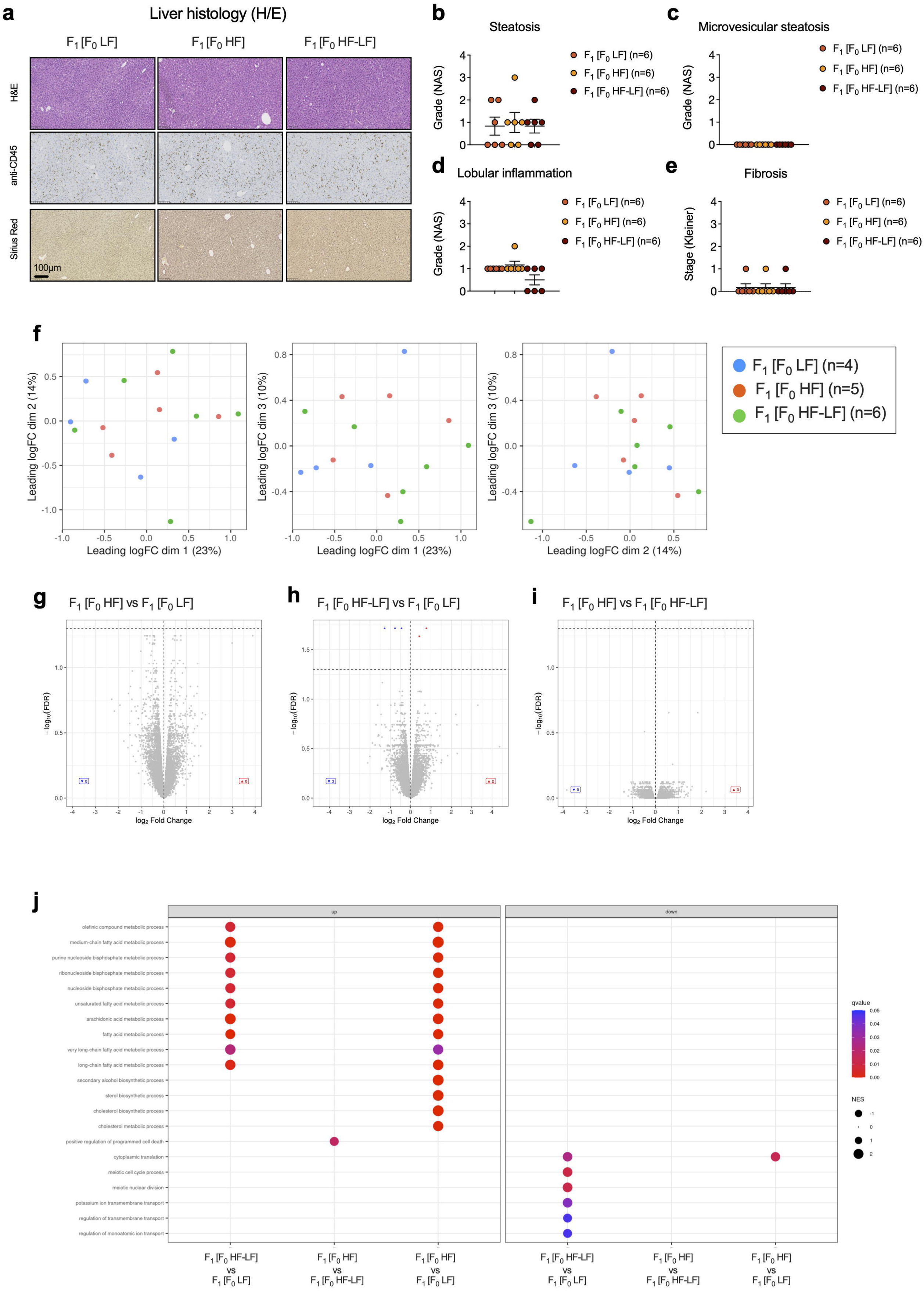

Figure S7: Reversible alterations in F_1 adipose mitochondria and identification of cross-generational miRNAs

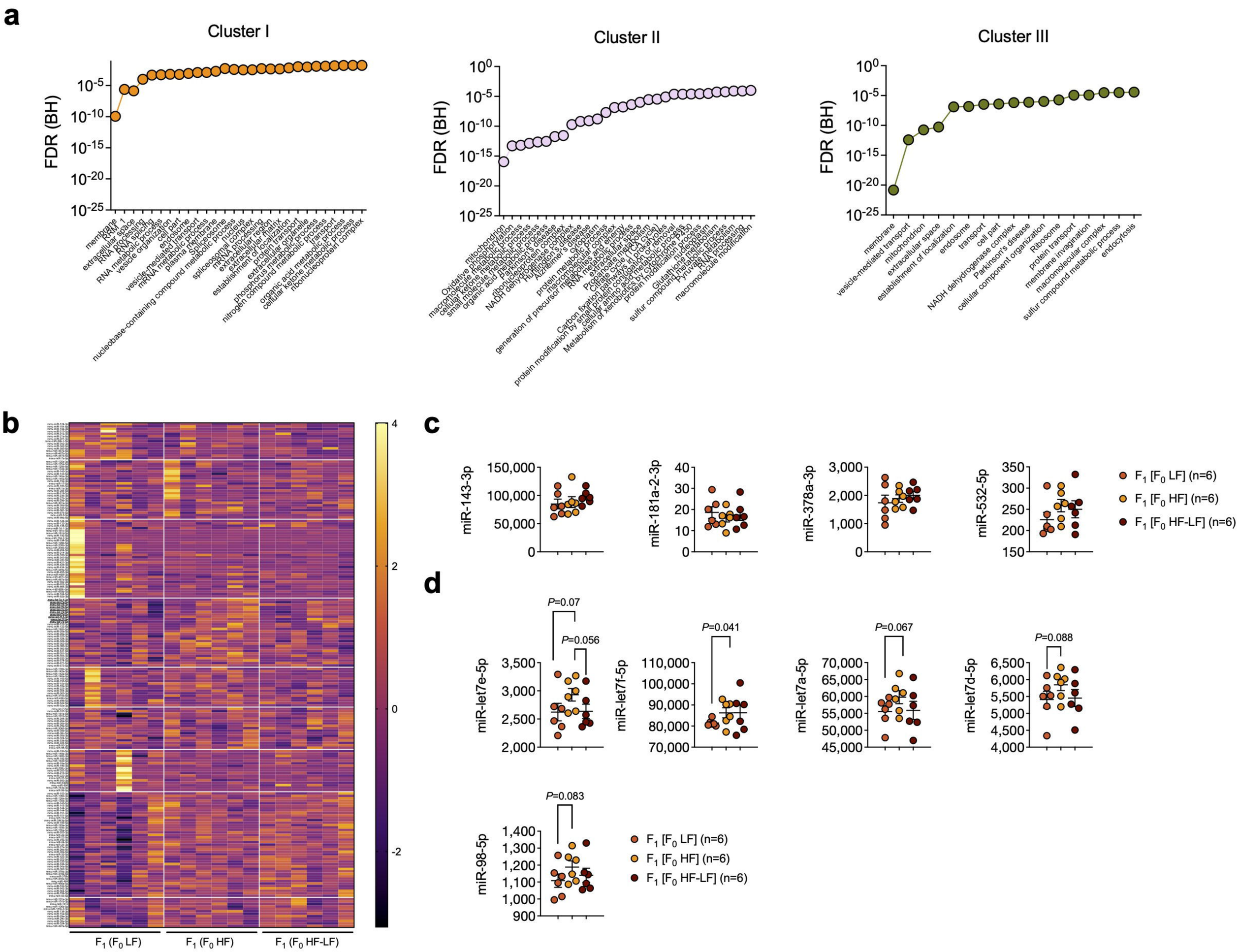
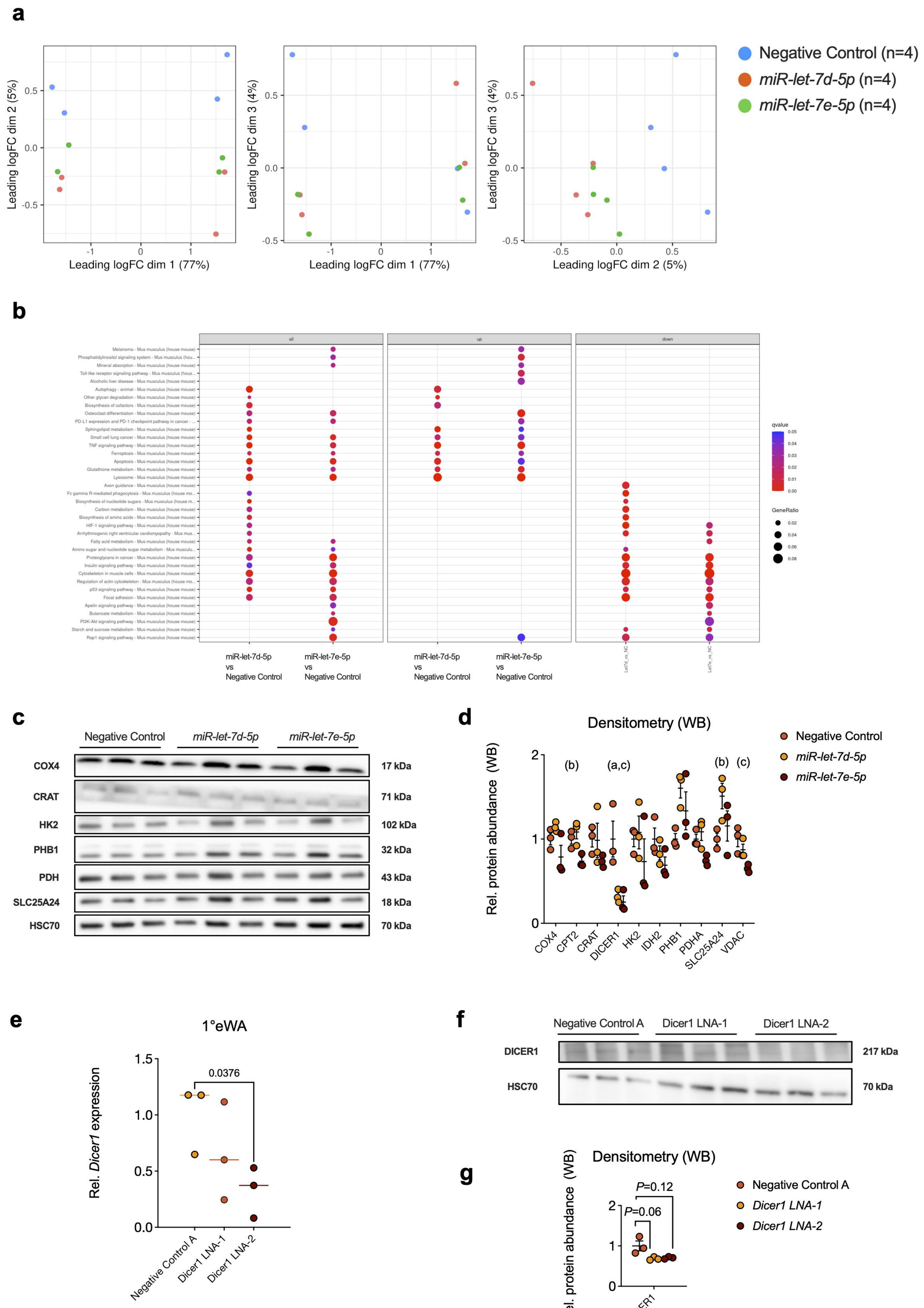
Figure S8: Obesity-associated miR-let-7 impairs adipocyte mitochondrial function via silencing of DICER1